Postprint of: Yang S., He Z., Chai J., Meng D., Macek W., Branco R., Zhu S., A novel hybrid adaptive framework for support vector machine-based reliability analysis: A comparative study, Structures Vol. 58 (2023), 105665, DOI: 10.1016/j.istruc.2023.105665

A novel hybrid adaptive framework for support vector machine-based reliability analysis: A comparative study

Shiyuan Yang[1, 2], Zhenyu He[1], Jiangbo Chai[1], Debiao Meng[1, 2, *], Wojciech Macek[3], Ricardo Branco[4], Shun-Peng Zhu[1, 2, *]

1. School of Mechanical and Electrical Engineering, University of Electronic Science and Technology of China, Chengdu, 611731, China

2. Institute of Electronic and Information Engineering of UESTC in Guangdong, Dongguan 523808, China

3. Gdansk University of Technology, Faculty of Mechanical Engineering and Ship Technology, 11/12 Gabriela Narutowicza, Gdansk 80-233, Poland

4. CEMMPRE, Department of Mechanical Engineering, University of Coimbra, 3030-788 Coimbra, Portugal

[*]Corresponding Author: dbmeng@uestc.edu.cn (D.B. Meng), zspeng2007@uestc.edu.cn (S.P. Zhu)

Telephone: 86-28-61830229

Fax: 86-28-61830227

Abstract

This study presents an innovative hybrid Adaptive Support Vector Machine - Monte Carlo Simulation (ASVM-MCS) framework for reliability analysis in complex engineering structures. These structures often involve highly nonlinear implicit functions, making traditional gradient-based first or second order reliability algorithms and Monte Carlo Simulation (MCS) time-consuming. The application of surrogate models has proven effective in addressing computational challenges associated with a large number of simulations. Support Vector Machine (SVM), as an emerging machine learning method suitable for small-sample scenarios, offers a well-established theoretical foundation and presents an effective model substitution approach for reliability analysis in engineering structures. However, the existing literature lacks a comprehensive and thorough comparative analysis of SVM's hybrid adaptive modeling

approach, encompassing initial sampling methods and learning functions, with regards to both computational efficiency and accuracy. Additionally, there is a gap in adaptive modeling methods capable of accommodating diverse types of input uncertainty, the nonlinearity of limit state functions, and various application scenarios. In response to these gaps, this article introduces the ASVM-MCS framework, which addresses these challenges by considering different types of input variables and various failure modes. Moreover, this study provides a comprehensive evaluation of the ASVM-MCS framework's performance, including its initial sampling methods and learning functions, across a range of application scenarios, such as scenarios involving only random variables, mixed variables, and the reliability of series-parallel systems.

Keywords Reliability analysis, Support vector machine, Monte Carlo simulation

Nomenclature

Symbols

$\boldsymbol{X}$	Input random variable
$f_X(x_1 \ldots x_n)$	The joint Probability Density Function (PDF)
$G(\boldsymbol{X})$	Limit State Function (LSF)
$\boldsymbol{\omega}$	Coefficient vector
$\boldsymbol{b}$	The constant of the hyperplane
λ_i	Lagrange multiplier
NSV	The number of support vectors
s	The category corresponding to the sample point $\boldsymbol{X}$
$K\left(\boldsymbol{X}_i, \boldsymbol{X}_j\right)$	Kernel function
$\mu_g(x)$	The predicted value at sample x
$\sigma_g(x)$	The standard deviation of the predicted values
d	Convergence threshold
m	The threshold of its LSF

$\boldsymbol{X}^c$	Test sample set
x^*	The updated sample selected by the learning function
$\varepsilon(x)$	The acceptable error of the distance to the boundary of the LSF
$\Phi(\bullet)$	The cumulative distribution function of normal distribution
$\phi(\bullet)$	The probability density function of normal distribution
g^+	The allowable upper limits of LSF
g^-	The allowable lower limits of LSF
r	The number of times to build SVR model
n	The number of LSF evaluations
P_f	Failure probability
δ	The deviation between the calculation results of the 9 combinations and the MCS calculation results
P_x	The lateral loads on the beam
P_y	The vertical loads on the beam
E	Elastic Modulus
D_0	Allowable displacement value
$[\varepsilon]$	The maximum deformation threshold
$\varepsilon_{\max}$	The actual maximum equivalent total deformation
$[\sigma]$	The yield strength of the structural steel
$\sigma_{\max}$	The actual maximum equivalent stress
$\boldsymbol{Y}$	Interval variable vector
$P_f^{\max}$	Maximum failure probability
k	The total number of failure modes in the system

$g_i(x)$ The LSF associated with the *i*th failure mode in the system

1 Introduction

When it comes to practical engineering applications, the process of reliability estimation involves computing the failure probability of for structure through the integral shown below:

$$P_f = P[G(\boldsymbol{X}) < 0] = \int \cdots \int_{G(\boldsymbol{X})<0} f_{\boldsymbol{X}}(x_1 \ldots x_n) \mathrm{d}x_1 \ldots \mathrm{d}x_n \quad (1)$$

where $\boldsymbol{X}$ is the input random variable. $f_{\boldsymbol{X}}(x_1 \ldots x_n)$ is the joint Probability Density Function (PDF). $G(\boldsymbol{X})$ is the Limit State Function (LSF). $G(\boldsymbol{X}) < 0$ indicates a failed state. Several methods have been developed to solve this integral, which can be broadly classified into three categories. The first category includes approximation methods like first-order reliability methods [1,2] and second-order reliability methods [3,4]. The second category consists of simulation-based methods, including direct Monte Carlo Simulation (MCS) [5,6], importance sampling [7,8], directional simulation [9,10], line sampling [11,12], and subset simulation [13]. The third category includes simulation methods based on surrogate models, such as response surface method [14,15], Support Vector Machine (SVM) [17-22] and Kriging model [23-31].

Aiming at the implicit functional function, the surrogate model and machine learning theory continue to develop [32-36]. For example, SVM, as an emerging small-sample machine learning method, has attracted more and more attention and research. Rocco and Moreno [37] used SVM to establish the feasibility of empirical models for reliability assessment. This approach exploits the fast computation capability of SVM, which is highly advantageous for performing a large number of model calculations commonly required for Monte Carlo reliability evaluation. Essentially, the method involves developing an estimation algorithm that can produce reasonably accurate model output by training the model on a limited dataset and replacing system performance evaluation with simpler calculations. SVM can be used not only for classification, but also for regression. Support Vector Regression (SVR) based on structural risk minimization is known for its excellent small-sample learning and generalization abilities, and is considered superior to traditional regression methods. However, when it comes to the reliability analysis of large samples, SVR can be time-consuming and space-intensive. To address these issues, Guo

and Bai [38] proposed the use of Least Squares SVM for Regression (LSSVR) in reliability analysis. Numerical results have demonstrated that the reliability analysis method based on LSSVR is more accurate and computationally efficient compared to the method based on SVM. A novel reliability method was developed by Pan and Daniel Dias [39] that uses adaptive SVM (ASVM) in conjunction with MCS. To minimize the number of training samples required, a learning function was proposed that sequentially selects informative training samples. The failure probability of the SVM-based classifier was then calculated using MCS. The performance of the proposed Adaptive Support Vector Machine - Monte Carlo simulation (ASVM-MCS) method was evaluated through four representative examples, demonstrating its high computational accuracy and efficiency. The method was found to provide an accurate estimation of the failure probability at a relatively low computational cost.

However, the above SVM-based reliability evaluation studies only consider the impact of random uncertainty. Due to a lack of samples, some parameters can only obtain variation intervals and cannot calculate accurate probability distributions, resulting in the final calculation of failure probability being also an interval. Therefore, studying probability interval mixed reliability analysis has very important engineering practical significance. Moreover, in practical engineering problems, there are often many failure modes, rather than just one. When conducting structural reliability analysis under multiple failure modes, it is necessary to consider the interaction between each failure mode. Therefore, studying system reliability analysis also has very important engineering practical significance.

To date, no comprehensive comparative study has been conducted on the hybrid adaptive modeling scheme of SVM models, which includes initial sampling methods and learning functions, with regard to computational efficiency and accuracy. Additionally, there is no single adaptive modeling method that can fully account for the various types of input uncertainty, as well as the nonlinearity of LHSs and application scenarios. Therefore, a hybrid ASVM-MCS framework is proposed in this article. This framework is able to consider different input variable types, different failure modes to conduct reliability evaluation. Furthermore, the performance of hybrid ASVM-MCS framework, including initial sampling methods and learning functions, is comprehensively studied in different application scenarios.

In the remaining part of this article, the second section discusses the basic principle of SVM, sampling method and learning function in detail. Furthermore, a general ASVM-MCS framework is proposed in this section. The Section 4 conducts the comparative study on hybrid ASVM-MCS framework considering random uncertainties, mixed uncertainties, and system reliability analysis. Finally, conclude this study in Section 5.

2 Review of theoretical knowledge

This section reviews some theoretical knowledge about SVM, sampling methods (Latin Hypercube Sampling (LHS), Halton low deviation sequence sampling, Round-Off sampling) and learning functions (U-learning, Expected Feasible Function (EFF), H-learning).

2.1 Support vector machines

The concept of SVM was initially proposed by Cortes and Vapnik [40] in 1995. This technique exhibits numerous advantages in areas such as small-sample, nonlinear, and high-dimensional pattern recognition. Additionally, its mathematical form is simple, its geometric interpretation is intuitive, and it offers good generalization capabilities. Compared with artificial neural networks, SVM can better solve the problems of over-learning and under-learning. In addition, it has a strong nonlinear classification ability. It is suitable for tasks such as classification and regression. SVM is extensively used in the field of pattern recognition. This algorithm converts the classification problem into a quadratic optimization problem, securing a global optimal solution that is independent of the specific sample point distribution.

In SVM theory, SVM classification mainly focuses on the binary classification solver. The purpose is to find a classification plane in the case of linearly separable samples:

$$\boldsymbol{\omega} \cdot \boldsymbol{X} + \boldsymbol{b} = 0 \tag{2}$$

This classification plane is called the optimal hyperplane, which aims to separate the two types of sample points correctly. Therefore, the core of the SVM classification algorithm is to try to find an optimal hyperplane as the classification boundary of the two groups of data and the minimum distance from the sample point closest to the hyperplane is the largest.

As shown in Figure 1, the blue triangles and red squares represent two types of sample points respectively. These two parallel dotted lines are defined as supporting hyperplanes, which

require at least one sample point in the two types of samples and there are no sample points within the interval of two parallel lines. The goal of the SVM classification algorithm is to determine such two parallel support hyperplanes to maximize the margin and then use the parallel midline as the optimal classification hyperplane. The sample points that pass the support hyperplane are defined as support vectors.

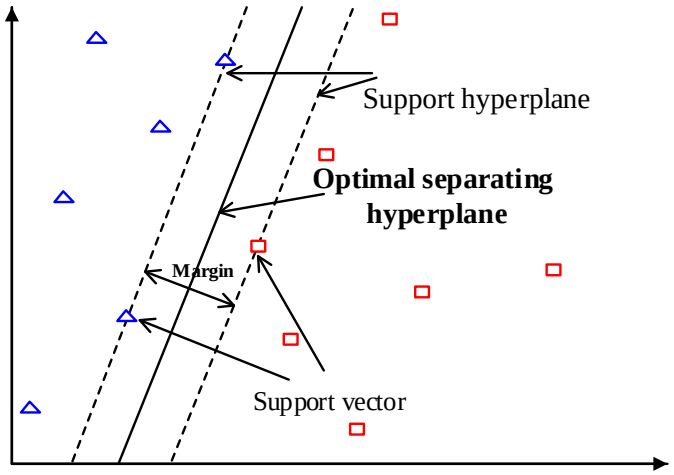

Figure. 1. Optimal classification hyperplane

The mathematical expression of the optimal hyperplane is:

$$\boldsymbol{\omega} \bullet \boldsymbol{X} + \boldsymbol{b} = 0 \tag{3}$$

The corresponding mathematical expression supporting the hyperplane is:

$$\begin{Bmatrix} \boldsymbol{\omega} \bullet \boldsymbol{X} + \boldsymbol{b} = +1 \\ \boldsymbol{\omega} \bullet \boldsymbol{X} + \boldsymbol{b} = -1 \end{Bmatrix} \tag{4}$$

where $\boldsymbol{\omega} \bullet \boldsymbol{X}$ is the inner product of two vectors in n-dimensional vector space. $\boldsymbol{X}$ is the vector of the sample point. $\boldsymbol{\omega}$ and $\boldsymbol{b}$ are the coefficient vector and constant of the hyperplane respectively. In order to satisfy that there are no sample points between parallel hyperplanes, it needs to satisfy:

$$\begin{Bmatrix} \boldsymbol{\omega} \bullet \boldsymbol{X}_i + \boldsymbol{b} \geq +1 & y = +1 \\ \boldsymbol{\omega} \bullet \boldsymbol{X}_i + \boldsymbol{b} \leq -1 & y = -1 \end{Bmatrix} \quad i = 1, 2, \ldots, N \tag{5}$$

Simplify the expression to get:

$$y_i \left[\left(\boldsymbol{\omega} \bullet \boldsymbol{X} + \boldsymbol{b} \right) \right] \geq +1 \quad i = 1, 2, \ldots, N \tag{6}$$

And the distance between two parallel planes is $\frac{2}{\|\boldsymbol{\omega}\|}$. In order to realize the correct classification of samples, it is necessary to determine the corresponding $\boldsymbol{\omega}$ and $\boldsymbol{b}$. For linearly separable data groups, the basic idea of SVM classification can be transformed into the following mathematical model:

$$\begin{aligned} &\min_{\boldsymbol{\omega},\boldsymbol{b}} \quad \frac{1}{2}\|\boldsymbol{\omega}\|^2 \\ &s.t.: \quad y_i\left(\boldsymbol{\omega} \bullet \boldsymbol{X} + \boldsymbol{b}\right) \geq +1 \quad 1 \leq i \leq N \end{aligned} \tag{7}$$

After solving by calculation tools such as MATLAB, the final classification calculation expression is obtained:

$$s = \operatorname{sgn}\left(\boldsymbol{b} + \sum_{i=1}^{N} \lambda_i y_i \boldsymbol{X}_i \boldsymbol{X}\right) \tag{8}$$

where λ_i is the Lagrange multiplier. Among all sample points, only the support vector satisfies $\lambda_i \neq 0$, so only support vectors have an effect on the constructed SVM model. The Eq. (8) can be expressed as:

$$s = \operatorname{sgn}\left(\boldsymbol{b} + \sum_{i=1}^{NSV} \lambda_i y_i \boldsymbol{X}_i \boldsymbol{X}\right) \tag{9}$$

where NSV is the number of support vectors. s is the category corresponding to the sample point $\boldsymbol{X}$.

Due to the limited classification ability of linear SVM, the classification results are often unsatisfactory for non-linearly separable sample points. The issue of nonlinearity in the SVM is addressed through the introduction of a crucial concept called kernel function. This function maps the input variables to a high-dimensional feature space using nonlinear transformation, after which the hyperplane is calculated in the feature space and projected back to the original space. The kernel function solves the problem of dimensionality disaster in reliability analysis well.

Nonlinear separable problems can be transformed into the following mathematical expressions:

$$s = \operatorname{sgn}\left(\boldsymbol{b} + \sum_{i=1}^{NSV} \lambda_i y_i \left\langle \phi\left(\boldsymbol{X}_i \right), \phi\left(\boldsymbol{X}_j \right) \right\rangle \right) = \operatorname{sgn}\left(\boldsymbol{b} + \sum_{i=1}^{NSV} \lambda_i y_i K\left(\boldsymbol{X}_i, \boldsymbol{X}_j \right) \right) \tag{10}$$

where $K\left(\boldsymbol{X}_i, \boldsymbol{X}_j \right)$ is the kernel function. For accuracy requirements and easy calculation, all examples in this paper will choose the most commonly used Gaussian kernel function for calculation.

2.2 Sampling method

In order to train a SVM model, an initial sample set must be obtained. Therefore, a sampling method that satisfies both the probability distribution function and is sufficiently dispersed and uniform must be considered, as it has a significant impact on the accuracy of the results. However, traditional uniformly distributed sampling is often insufficient to meet the requirements of agent-based model reliability analysis. Therefore, this section will introduce three sampling methods, such as LHS, Halton low deviation sequence sampling, and round-off sampling. These three sampling methods are more effective.

2.2.1 Latin hypercube sampling

LHS is a multidimensional random sampling method used to generate sample points in a multidimensional parameter space. The steps are as follows:

(1) Determine the number of dimensions of the parameter space and the number of sample points and divide the parameter space of each dimension into equal intervals.

(2) A Latin hypercube matrix of size n × m is generated, where n is the dimensionality of the parameter space and m is the number of sample points. Each row of the Latin hypercube matrix represents the interval in which a sample point is located in each parameter dimension.

(3) A point in each interval is chosen at random as the value of the sample point.

(4) Repeat step (3) until the values of all sample points are generated. Use all the resulting sample points as input for subsequent calculations or analysis.

LHS can effectively avoid the aggregation phenomenon in the multidimensional parameter space, improving the efficiency and quality of sampling.

2.2.2 Halton low bias sequence sampling

Halton low discrepancy sequence sampling is a multi-dimensional random sampling method used to generate sample points in a multi-dimensional parameter space [41]. The steps are as follows:

(1) Select a different set of prime numbers as the base of the Halton sequence. Map the parameter space of each dimension onto the interval [0,1] and divide it into equal intervals.

(2) Generate a Halton sequence of size n × m, where n is the dimensionality of the parameter space and m is the number of sample points. each row of the Halton sequence represents the value of a sample point in each parameter dimension, a fraction between 0 and 1.

(3) Each score is mapped back to the original parameter space to obtain the actual value of each sample point in each parameter dimension.

(4) Repeat step (3) until the fetch values for all sample points are generated. Use all the resulting sample points as input for subsequent calculations or analysis.

Halton low bias sequential sampling is also effective in avoiding "aggregation" in multi-dimensional parameter spaces, improving sampling efficiency and sampling quality. Halton sequences have lower bias and higher homogeneity than LHS, and are therefore more suitable in certain situations.

2.2.3 Round-off sampling

Round-Off Sampling (ROS) is a random sampling method used to generate a sample from a distribution with a complex probability density function. The steps are as follows:

(1) Set a repeatable simple probability distribution (such as a uniform or normal distribution) whose support set must contain the support set of the target distribution.

(2) Take a sample point under the simple probability distribution and calculate the ratio of the value of the probability density function for that point under the target distribution to the value of the probability density function under the simple probability distribution, denoted as r.

(3) Generate a uniformly distributed random number u in the interval [0,1] and accept the sample point if u is less than or equal to r, otherwise reject the sample point.

(4) Repeat steps (2) and steps (3) until a sufficient number of sample points have been generated. Treat all accepted sample points as samples drawn from the target distribution.

The advantages of ROS are that it is widely applicable, can be applied to a variety of target distributions and can be computed in parallel. The disadvantage is that a simple probability distribution needs to be found and the support set of that distribution must contain the support set of the target distribution, otherwise the sampling efficiency will be reduced. In addition, ROS may also suffer from low acceptance rates, resulting in the need to generate a large number of sample points to obtain a sufficient number of valid samples.

2.2.4 Effect comparison

In order to demonstrate the sampling effect, the above three methods and the common uniform sampling method are compared with sampling of 100 sample points each. The sampling results are shown in Figure 2:

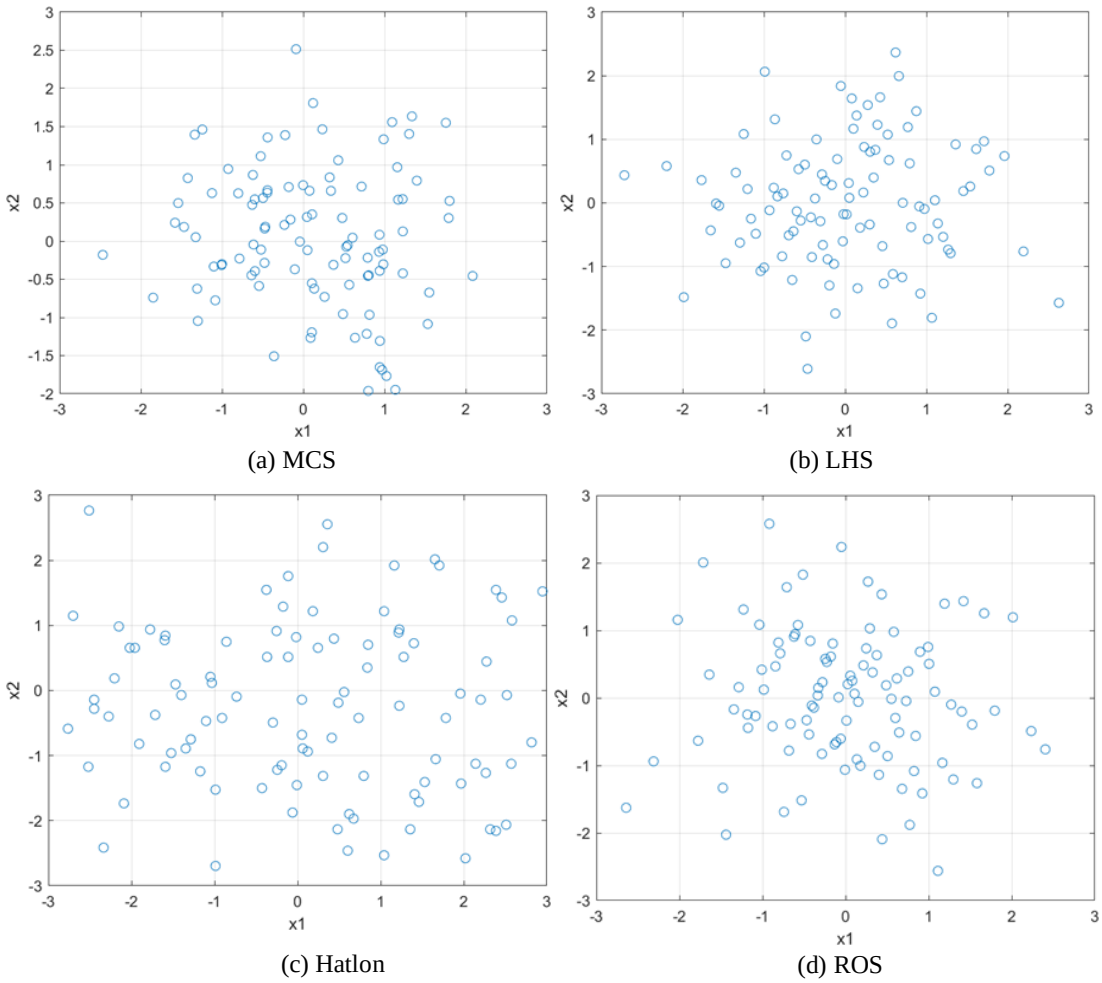

(a) MCS (b) LHS

(c) Hatlon (d) ROS

Figure. 2. Comparison of Sampling Methods (a) MCS, (b) LHS, (c) Halton, (d) ROS

It can be seen from Figure 2 that the sampling effect of Halton low-bias sequence is more uniform than that of the other three. In this method, there are fewer overlapping sample points, indicating that it is a better method.

2.3 Learning function

The crux of modeling lies in utilizing available sample information to identify the sample that contributes most significantly to the learning scheme for constructing the model. In conventional modeling, the sample that has the most significant contribution is typically indicative of the highest level of uncertainty in the predicted value. When the prediction accuracy is high, the reliability estimation outcome based on the surrogate model is also expected to be more precise. To curtail the number of actual experiments or the simulated sample size, greater emphasis is placed on samples that have the most significant contribution to failure probability solution. Attention is particularly focused on whether the prediction point crosses the failure boundary, i.e., the accuracy of positive or negative judgment of the LSF value. In this section, three learning functions will be presented, namely U-learning, Expected Feasibility Function (EFF), and H-learning. The learning function will update specific sample points to optimize the SVM.

2.3.1 U-learning

U-learning was proposed by Echard et al. [42] based on the probability hypothesis testing theory, which can be expressed as a mathematical expression as follows:

$$U\left(x\right)=\left|\frac{\mu_g\left(x\right)-m}{\sigma_g\left(x\right)}\right| \tag{11}$$

where $\mu_g\left(x\right)$ is the predicted value at sample x. $\sigma_g\left(x\right)$ is the standard deviation of the predicted values. m is the threshold of its LSF. In this paper $m=0$. Assume that the threshold m is within k times standard deviations of the predicted value. According to the characteristics of the PDF of the normal distribution, the smaller the value k, the more likely it is to pass through the failure surface and lead to misjudgment of failure. Therefore, the learning scheme in U-learning is defined as:

$$x^* = \arg\min\left(U\left(\boldsymbol{X}^c\right)\right) \tag{12}$$

where $\boldsymbol{X}^c$ is the test sample set. x^* is the updated sample selected by the learning function. The corresponding stopping criteria are:

$$\min\left(U\left(\boldsymbol{X}^c\right)\right) \geq d \tag{13}$$

where d represents the convergence threshold.

2.3.2 EFF

The fundamental idea of EFF [43] is to evaluate if a sample is probable to surpass the limit failure boundary, considering the weighted distance between the sample and the failure boundary. This can be mathematically represented as:

$$\begin{aligned} EFF\left(x\right) &= \int_{m-\varepsilon(x)}^{m+\varepsilon(x)} \left[\varepsilon\left(x\right) - \left|m-g\right|\right] f\left(g\left(x\right)\right) dg\left(x\right) \\ &= \left[\mu_g\left(x\right) - m\right]\left[-\Phi\left(\tau^-\left(x\right)\right) - \Phi\left(\tau^+\left(x\right)\right)\right] + 2\sigma_g\left(x\right)\Phi\left(\tau^+\left(x\right)\right) \\ &\quad - 2\sigma_g\left(x\right)\Phi\left(\tau^-\left(x\right)\right) + 2\left[\mu_g\left(x\right) - m\right]\Phi\left(\frac{g-\mu_g\left(x\right)}{\sigma_g\left(x\right)}\right) \\ &\quad - 2\sigma_g\left(x\right)\phi\left(\frac{g-\mu_g\left(x\right)}{\sigma_g\left(x\right)}\right) + \sigma_g\left(x\right)\left[\phi\left(\tau^-\left(x\right)\right) + \phi\left(\tau^+\left(x\right)\right)\right] \end{aligned} \tag{14}$$

$$\tau^+\left(x\right) = \frac{g^+ - \mu_g\left(x\right)}{\sigma_g\left(x\right)} \tag{15}$$

$$\tau^-\left(x\right) = \frac{g^- - \mu_g\left(x\right)}{\sigma_g\left(x\right)} \tag{16}$$

where m is the threshold of the LSF. $\varepsilon\left(x\right)$ represents the acceptable error of the distance to the boundary of the LSF. $\varepsilon\left(x\right) - \left|m-g\right|$ is the distance between the specimen and the acceptable boundary of the LSF. $g^+ = m + \varepsilon\left(x\right)$, $g^- = m - \varepsilon\left(x\right)$ and $\Phi\left(\bullet\right)$ is the cumulative distribution function of a standard normally distributed variable, $\phi\left(\bullet\right)$ is the corresponding PDF. In this article, $m = 0$ and $\varepsilon\left(x\right) = 2\sigma_g\left(x\right)$. The learning scheme in EFF is expressed as:

$$x^* = \arg\max\left(EFF\left(\boldsymbol{X}^c\right)\right) \tag{17}$$

The mathematical expression for the stopping criterion is:

$$\max\left(EFF\left(\boldsymbol{X}^{c}\right)\right)\le d \tag{18}$$

2.3.3 H-learning

H-learning was proposed by Lv et al [44]. based on the principle of information entropy. The principle can be expressed as:

$$\begin{aligned} H(x) &= \left|-\int_{g^-}^{g^+} f_g\left(g(x)\right)\ln f_g\left(g(x)\right)dg(x)\right| \\ &= \left|\begin{array}{l} -\alpha(x)\phi\left(\alpha(x)\right)-\alpha(x)\phi\left(\alpha(x)-4\right) \\ +\ln\left(\sqrt{2\pi}\sigma_g(x)+\frac{1}{2}\right)\Phi\left(\alpha(x)\right)-\ln\left(\sqrt{2\pi}\sigma_g(x)+\frac{1}{2}\right)\Phi\left(\alpha(x)-4\right) \end{array}\right| \end{aligned} \tag{19}$$

$$\alpha(x)=\frac{2\sigma_g(x)-\mu_g(x)}{\sigma_g(x)} \tag{20}$$

where g^+ and g^- are the allowable upper and lower limits of LSF, respectively. $g^+=m+\varepsilon(x)$ and $g^-=m-\varepsilon(x)$. In this paper, $m=0$, $\varepsilon(x)=2\sigma_g(x)$. The learning scheme for selecting and updating samples is expressed as:

$$x^{*}=\arg\max\left(H\left(\boldsymbol{X}^{c}\right)\right) \tag{21}$$

This implies that every chosen sample has the highest level of uncertainty. Furthermore, the stopping criterion is expressed as:

$$\max\left(H\left(\boldsymbol{X}^{c}\right)\right)\le d \tag{22}$$

3 The proposed ASVM-MCS framework

3.1 The ASVM-MCS framework considering random uncertainties

The basic steps of the overall framework of the hybrid ASVM-MCS in this article are as follows, which can be represented by the following Figure 3:

Step1: Generate initial training samples. Some sampling methods in Section 2.2 can be used to generating initial training sample. Then evaluate the actual response of these samples. Furthermore, set the number of times to build SVR model r=0.

Step2: Build or rebuild SVM model. If r=0, build SVR model by initial training samples. Else, add updated sample to training samples rebuild SVR model by these new training samples.

Step3: Pick a new updated sample. Generate candidate test sample by some sampling methods in Section 2.2. Some learning function in Section 2.3 can be used to pick a new updated sample. Then calculate the actual response of the picked sample. It is worth noting that the kriging variance used in the learning function here is replaced by the jackknife variance [45].

Step4: SVM model accuracy judgment. Determine whether the model accuracy meets the requirements based on different learning function convergence conditions. If the requirements are met, go to **Step** 5. Otherwise, return to **Step** 2.

Step5: Reliability evaluation. First, generate Monte Carlo samples. Then use the constructed SVM model to evaluate the response value of the sample. Finally, this response sample is used to estimate the probability of failure.

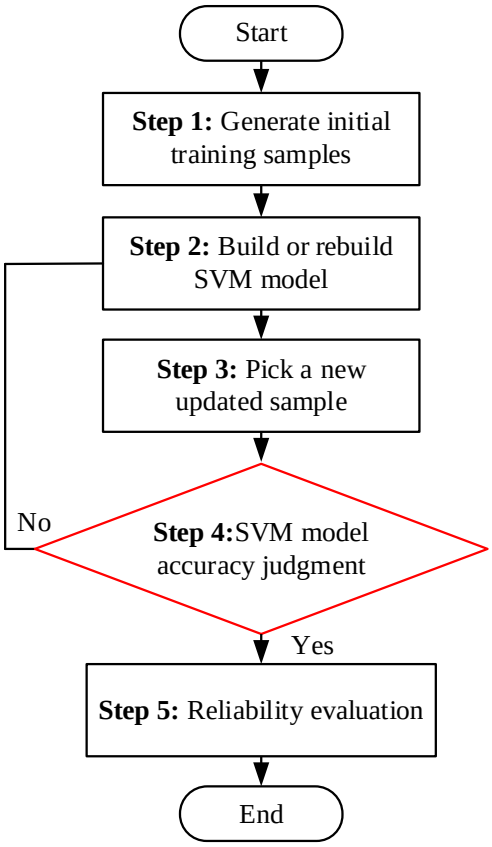

Figure. 3. Flowchart of the hybrid ASVM-MCS framework

3.2 The ASVM-MCS framework considering mixed uncertainties

In practical engineering, uncertainty is divided into random uncertainty and cognitive uncertainty. Probability and interval information are used to describe these two uncertainties, respectively. When the structure contains both probability variables and interval variables, the

related functional expression can be described as:

$$Z = g(\boldsymbol{X}, \boldsymbol{Y}) \tag{23}$$

where $\boldsymbol{X} = (X_1, X_2, ..., X_m)$ is a n dimensional interval vector:

$$P_f = P_r\{g(\boldsymbol{X}, \boldsymbol{Y}) \le 0\} \tag{24}$$

After the interval variable $\boldsymbol{Y}$ is introduced, the limit state $g(\boldsymbol{X}, \boldsymbol{Y}) = 0$ is no longer the only surface in the space, but a limit state zone composed of two boundary surfaces $\max_{Y} g(\boldsymbol{X}, \boldsymbol{Y}) = 0$ and $\min_{Y} g(\boldsymbol{X}, \boldsymbol{Y}) = 0$. Therefore, the failure probability P_f also has upper and lower bounds, expressed as:

$$\begin{aligned} P_f^{\min} &= \Pr\{\max_{Y} g(\boldsymbol{X}, \boldsymbol{Y}) \le 0\} \\ P_f^{\max} &= \Pr\{\min_{Y} g(\boldsymbol{X}, \boldsymbol{Y}) \le 0\} \end{aligned} \tag{25}$$

In practical engineering, the maximum failure probability of structures is typically the most important and highly-regarded index. Therefore, to evaluate the reliability of the mixed uncertainty structure in the subsequent analysis of this paper, the maximum failure probability $P_f^{\max}$ will be utilized.

The proposed ASVM-MCS framework considering mixed uncertainties is similar to the method that only considers random uncertainties. The only difference is in the reliability assessment step. In a framework that considers mixed uncertainties, the hybrid reliability method based on projection outline proposed by Zhang et al. [46] is used to evaluate reliability.

3.3 System reliability analysis based ASVM-MCS framework

In the structural reliability problem with multiple failure modes, when the failure modes of the system are connected in parallel, the failure probability can be expressed as:

$$P_f = P\left\{\bigcap_{i=1}^{k} g_i(x) < 0\right\} = P\left\{\max_{i=1}^{k} g_i(x) < 0\right\} \tag{26}$$

where k denotes the total number of failure modes in the system. $g_i(x)$ represents the LSF associated with the ith failure mode in the system. It is worth noting that the entire system will only fail if all the failure modes in the parallel system fail simultaneously. Conversely, if there is

a failure mode in the system that remains functional, the system can still be considered safe. Thus, the failure mode with the highest value of the function in the system determines the failure probability of the entire parallel system.

Similarly, when the failure modes in the system are connected in series, the failure probability is:

$$P_f = P\left\{\bigcup_{i=1}^{k} g_i(x) < 0\right\} = P\left\{\min_{i=1}^{k} g_i(x) < 0\right\} \tag{27}$$

It can be found that if one failure mode fails in the system, the whole system will fail. A system is in a safe state only when all failure modes are not failed. For a series system, the failure mode with the lowest value of the function determines the probability of failure of the system.

On the basis of Section 3.1, the ASVM-MCS framework in system reliability requires separate optimization for each branch before MCS calculation due to the presence of multiple functional functions. Then conduct reliability analysis according to the classification of series and parallel connections.

4 Results and discussion

In this section, the proposed ASVM-MCS framework is comprehensively compared. Once a sufficient number of samples are available, the result of the MCS calculation will be almost identical to the actual failure probability. Therefore, MCS method is used to evaluate the accuracy of different combination in this study. Furthermore, the calculation results of the number of iterations and failure probability are the average of 10 calculation results to reduce the contingency of the experiment.

4.1 Numerical examples for the comparative study on hybrid ASVM-MCS framework considering random uncertainties

In order to further investigate the impact of the proposed framework considering random uncertainties on the performance of different structures, six examples are selected, including two benchmark numerical examples and two engineering examples. Estimate accuracy and efficiency through corresponding calculation results.

4.1.1 Nonlinear function

Since linear classification is relatively simple for the SVM model, a nonlinear function is used to verify the performance of the model. The LHS can be taken as the following mathematical expression:

$$f\left(x_1, x_2\right) = 3 - 0.1x_1^3 - x_2 \tag{28}$$

where x_1, x_2 all obey the standard normal distribution and are independent of each other. The calculation results are shown in Table 1. The iteration diagram and boxplot of the failure probability are shown in Figure 4 and Figure 5 respectively:

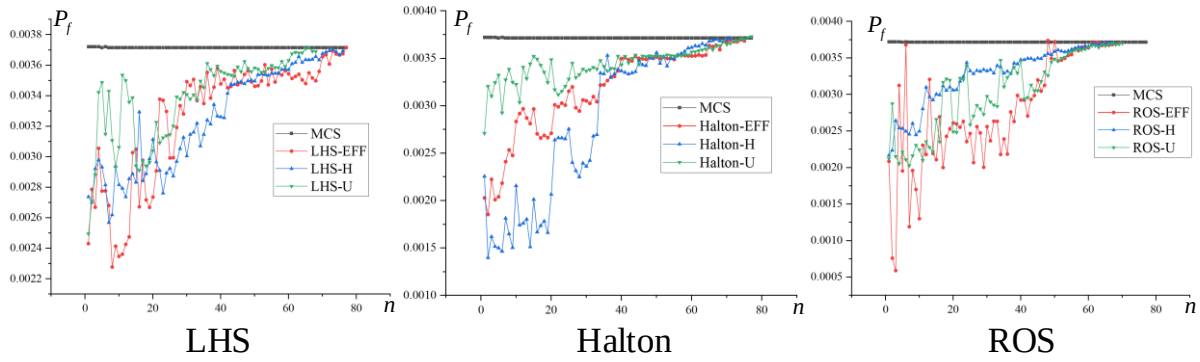

Figure. 4. Failure probability iterative diagram in example 1

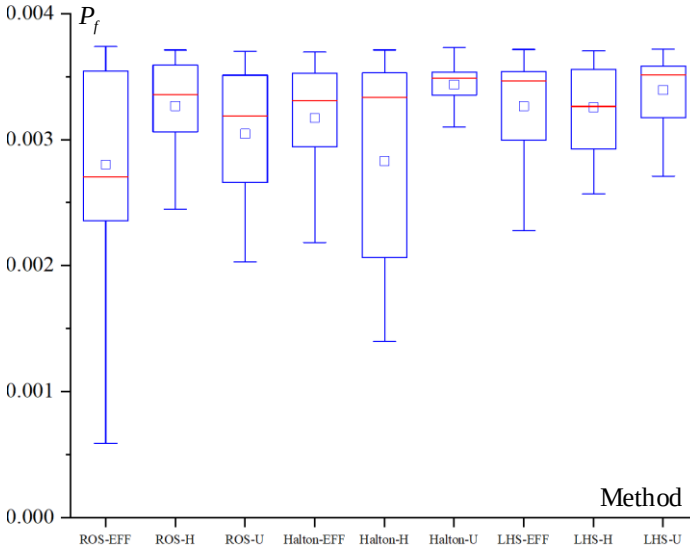

Figure. 5. Failure probability boxplot in example 1

Table 1 Calculation results of nonlinear function example considering random uncertainties

Method	n	P_f	δ / %	**Method**	n	P_f	δ / %

MCS	2×10^6	0.003701	0	Halton-U	12+76	0.003681	0.54
LHS-H	12+79	0.003716	0.40	Halton-EFF	12+73	0.003711	0.27
LHS-U	12+77	0.003683	0.49	ROS-H	12+73	0.003675	0.70
LHS-EFF	12+81	0.003690	0.30	ROS-U	12+78	0.003679	0.60
Halton -H	12+71	0.003669	0.86	ROS-EFF	12+75	0.003693	0.22

In the Table 1, n represents the number of LSF evaluations. P_f represents the failure probability. δ represents the deviation between the calculation results of the 9 combinations and the MCS calculation results. It is worth noting that these symbols have the same meaning in the subsequent tables.

It can be seen from Figure 4 that the failure probabilities calculated by all combinations gradually approach MCS with the iteration of the learning function, which shows that the learning function does optimize the SVM model and ASVM does have a good effect on reliability analysis. According to the comparison of the results in Table 1, if only the learning function is compared, it can be seen that the calculation accuracy corresponding to the EFF function is the highest and the number of iterations is the least. If only the sampling methods are compared, it can be seen that Halton's low deviation sequence sampling corresponds to the highest computational accuracy and the least number of iterations. Comprehensively comparing all the data, Halton-EFF is the combination with the best performance in this example.

4.1.2 Highly nonlinear function

The mathematical expression of a highly nonlinear function is as follows:

$$y = 1 + 1/256(x_1 + x_2 - 10)^4 - 10/(x_1 + x_2) \tag{29}$$

where $x_1 \in N(10,3)$, and $x_2 \in N(10,3)$. The calculation results are shown in Table 2, and the iteration plot and box plot of the failure probability are shown in Figure 6 and Figure 7, respectively.

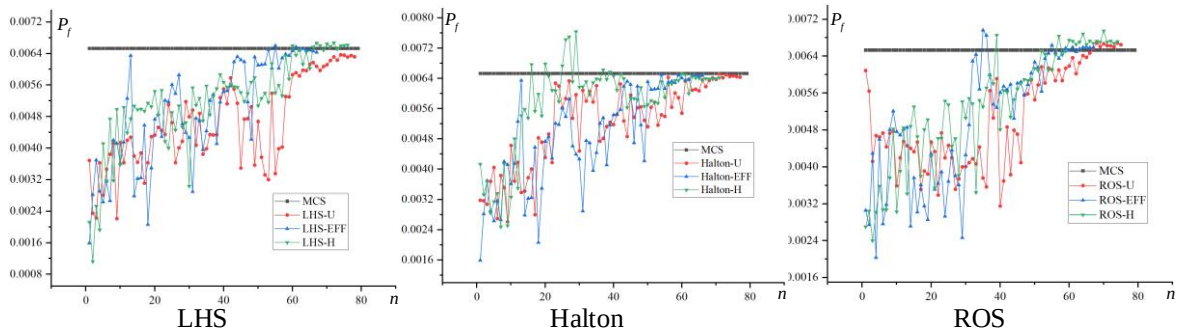

Figure. 6. Failure probability iterative diagram in example 2

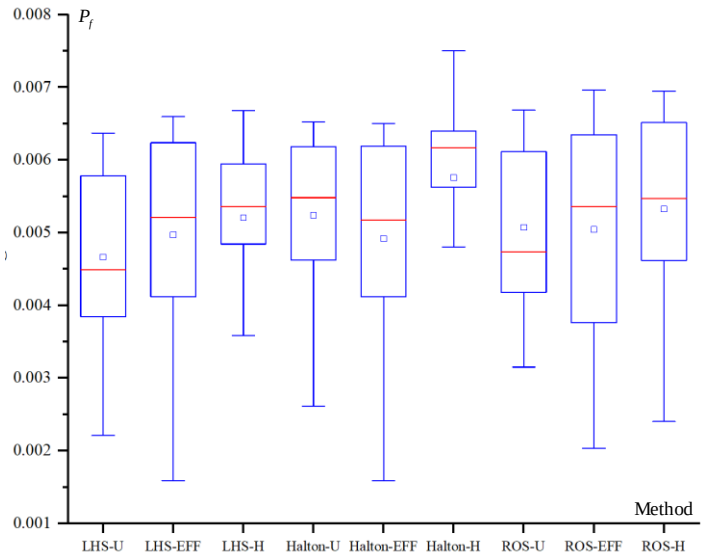

Figure. 7. Failure probability boxplot in example 2

Table 2 Calculation results of highly nonlinear function example considering random uncertainties

Method	n	P_f	δ / %	**Method**	n	P_f	δ / %
MCS	2×10^6	0.006533	0	Halton-U	12+77	0.006437	1.49
LHS-H	12+76	0.006619	1.30	Halton-EFF	12+66	0.006475	0.89
LHS-U	12+78	0.006320	3.26	ROS-H	12+74	0.006720	2.86
LHS-EFF	12+67	0.006433	1.53	ROS-U	12+75	0.006650	1.79
Halton -H	12+71	0.006418	1.76	ROS-EFF	12+67	0.006590	0.87

It can be seen from Figure 6 that the increase in the degree of nonlinearity does not affect ASVM, and the calculation results are still slowly approaching MCS. It can be seen from Table 2 that the overall calculation error has a certain increase compared with Table 1, but the accuracy is still reliable. If only the sampling method is compared, the Halton low-bias sequence sampling

has the highest precision and the fastest efficiency; if only the learning function is compared, the EFF function has the highest precision and the fastest efficiency; comprehensive comparison shows that the Halton-EFF combination has the best performance.

4.1.3 High-dimensional nonlinear functions

Since SVM has certain advantages in high-dimensional function calculation examples, a high-dimensional calculation example is test in this study. The following formula is a twenty-dimensional LSF:

$$f(x)=\sum_{i=1}^{19}\left[2(x_{i+1}-x_i^2)^2+0.5(x_i-1)^2\right]-700 \tag{30}$$

where $x_1, x_2, ..., x_{20}$ all obey the standard normal distribution and are independent of each other. The calculation results are shown in Table 3. The iteration diagram and box plot of the failure probability are shown in Figure 8 and Figure 9 respectively.

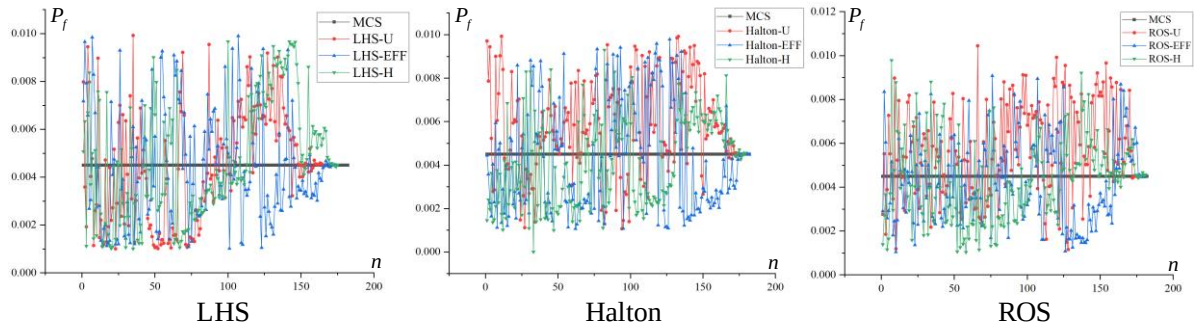

Figure. 8. Failure probability iterative diagram in example 3

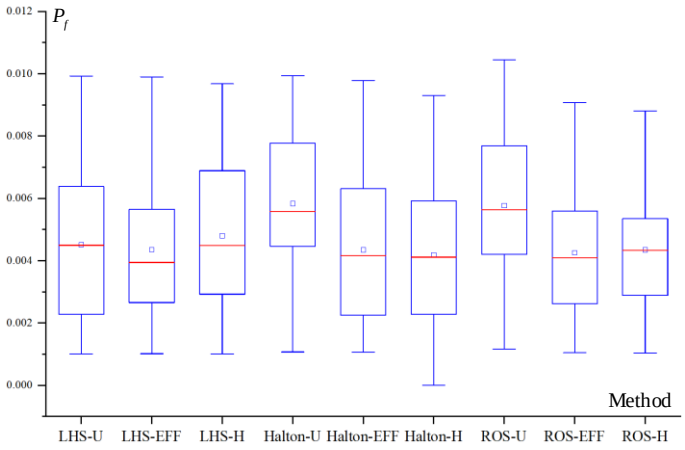

Figure. 9. Failure probability boxplot in example 3

Table 3 Calculation results of high-dimensional nonlinear function example considering random

uncertainties

Method	n	P_f	δ / %	Method	n	P_f	δ / %
MCS	2×10^6	0.004500	0	Halton-U	20+177	0.004471	0.64
LHS-H	20+175	0.004522	0.49	Halton -EFF	20+182	0.004486	0.31
LHS-U	20+166	0.004478	0.49	ROS-H	20+181	0.004585	1.90
LHS-EFF	20+174	0.004505	0.11	ROS-U	20+176	0.004445	1.20
Halton -H	20+179	0.004548	1.10	ROS-EFF	20+180	0.004461	0.87

As shown in Figure 8, Although the calculation results of the failure probability of each combination fluctuate significantly, they still converge slowly near the MCS in the end. It shows that the learning function still has a certain optimization effect, but the effect of optimization on high-dimensional calculation examples is not obvious. According to the comparison of the results in Table 2, If only the learning function is compared, it can be seen that the calculation accuracy of the corresponding combination of the EFF function is the highest and the number of iterations is the least; If only the sampling method is compared, it can be seen that the calculation accuracy of the combination corresponding to LHS is the highest and the number of iterations is the least; Comprehensively comparing all the data, LHS-EFF is the combination with the best performance in this high-dimensional example.

4.1.4 Cantilever beam

Figure 10 is a schematic structural diagram of a cantilever beam. The LSF $G(\bullet)$ [18] is considered by a displacement of allowable value D_0 under both loads P_x and P_y in this example, which can be calculated by Eq. (31). Furthermore, P_x and P_y are applied to the free end of the beam in Figure 10. It is important to note that these external loads are applied to the free end of the cantilever beam.

$$G(D_0, L, E, w, t, P_x, P_y) = D_0 - \frac{4L^3}{Ewt}\sqrt{\left(\frac{P_x}{w^2}\right)^2 + \left(\frac{P_y}{t^2}\right)^2} \tag{31}$$

where the meanings and distribution of random variables are shown in Table 4. The calculation results are shown in Table 5. The iteration diagram and box plot of the failure probability are shown in Figure 11 and Figure 12, respectively.

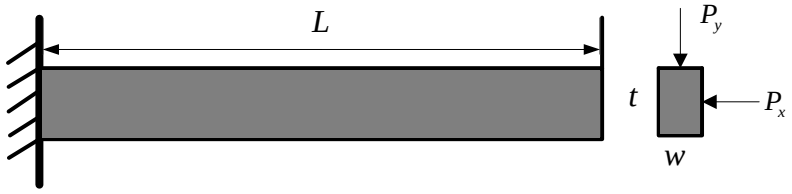

Figure. 10. Schematic diagram of cantilever beam structure

Table 4 Variable distribution of cantilever beam engineering example

Variables	Distribution	Mean	Standard deviation
Allowable displacement value D_0	Lognormal	3	0.3
Elastic Modulus E	Normal	3×10^7	1×10^6
length of cantilever beam L	Normal	100	10
The width of the cantilever beam section w	Normal	2	0.25
The height of the cantilever beam section t	Normal	4	0.4
The lateral loads on the beam P_x	Normal	100	20
The vertical loads on the beam P_y	Normal	200	20

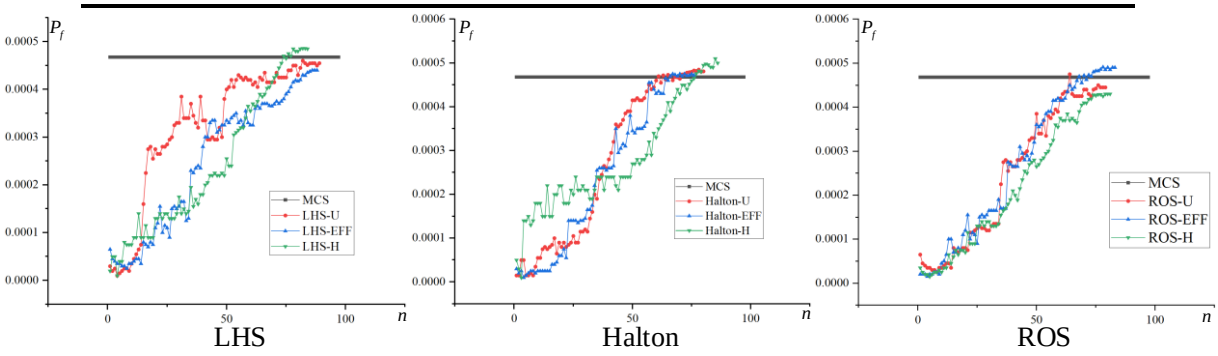

Figure. 11. Failure probability iteration diagram of cantilever beam engineering example

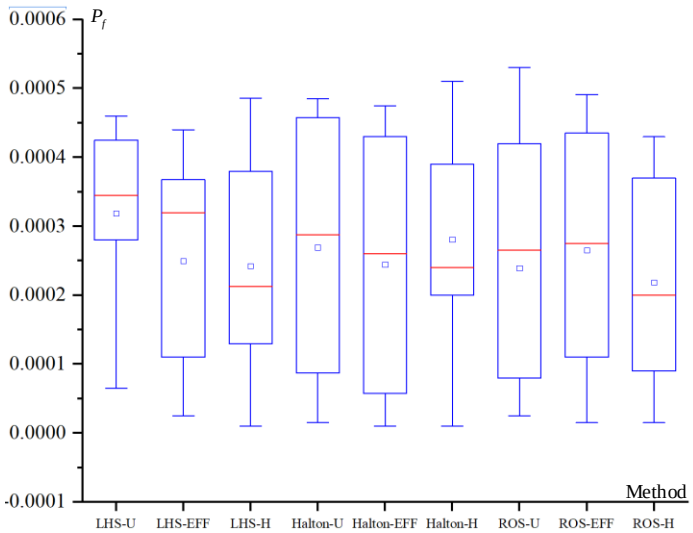

Figure. 12. Boxplot of failure probability of cantilever beam engineering example

Table 5 Calculation results of cantilever beam engineering example considering random uncertainties

Method	n	P_f	δ / %	Method	n	P_f	δ / %
MCS	2×10^6	0.000467	0	Halton-U	12+80	0.000481	3.00
LHS-H	12+84	0.000485	3.85	Halton-EFF	12+76	0.000472	1.07
LHS-U	12+89	0.000455	2.60	ROS-H	12+81	0.000430	7.92
LHS-EFF	12+88	0.000441	5.56	ROS-U	12+79	0.000445	4.71
Halton -H	12+86	0.000502	7.49	ROS-EFF	12+83	0.000490	4.92

As shown in Figure 11, the calculation results of the failure probabilities of each combination converge regularly around the MCS from small to large. It shows that the learning function also plays a certain role in engineering practice. According to the comparison of the results in Table 5, if only the learning function is compared, it can be seen that the calculation accuracy of the combination corresponding to the EFF function is the highest and the number of iterations is the least. If only the sampling methods are compared, it can be seen that the calculation accuracy of the combination corresponding to Halton low-difference sequence sampling is the highest and the number of iterations is the least. Comprehensively comparing all the data, it is considered that Halton -EFF has the best performance in this engineering example combination.

4.1.5 Support bracket

This example is a static simulation. As shown in Figure 13, it is a supporting bracket in an aircraft braking structure, which plays an important role in the braking system. The material is structural steel. The triangular ribs in the middle increase the strength of the structure. In order to simulate the actual engineering, a fixed support is applied to the square tube and a vertical force of 500N is applied to the edge of the steel plate below. The results obtained by finite element simulation analysis are shown in Figure 14. In this calculation example, the length L, width H and thickness D of the ribs are taken as three independent random variables and the distribution rules are shown in Table 6. The corresponding LHS is as follows:

$$G(L,H,D)=[\varepsilon]-\varepsilon_{\max}(L,H,D) \tag{32}$$

where $[\varepsilon]$ is the maximum deformation threshold. $\varepsilon_{\max}$ represents the actual maximum equivalent total deformation, which is an implicit function of L,H,D. The unit of $\varepsilon_{\max}$ is $10^{-6}m$.

The calculation results are shown in Table 7. The iteration plot and box plot of the failure probability are shown in Figure 15 and Figure 16 respectively.

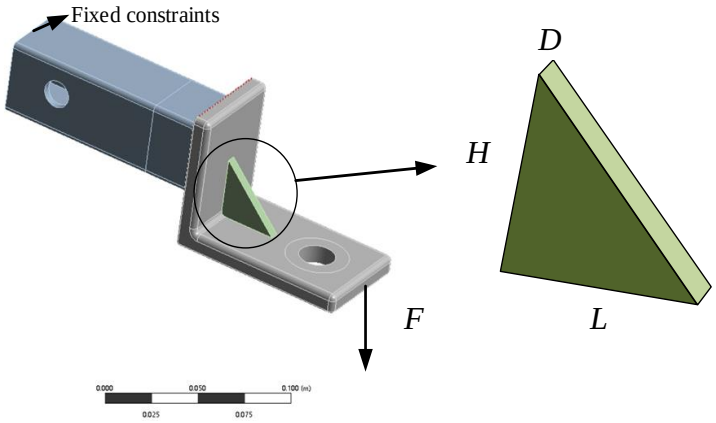

Figure. 13. Support bracket

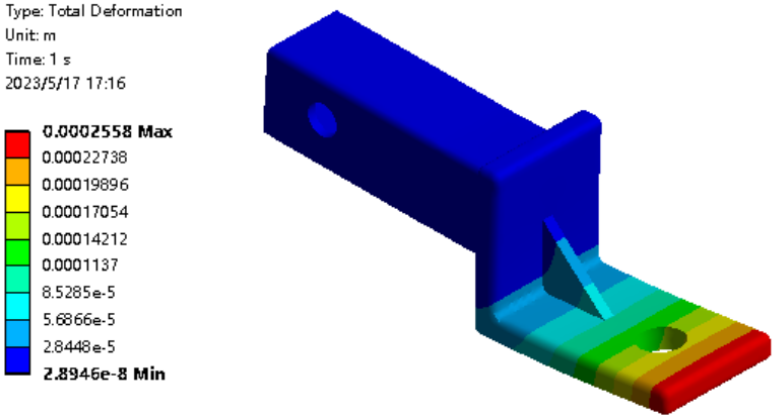

Figure. 14. ANSYS simulation results

Table 6 Variable information of supporting bracket example

Variable	Distribution	Mean	Standard deviation
Rib length *L*/mm	Normal	30	1
Rib width *H*/mm	Normal	30	1
Rib thickness *D*/mm	Normal	2.5	0.1

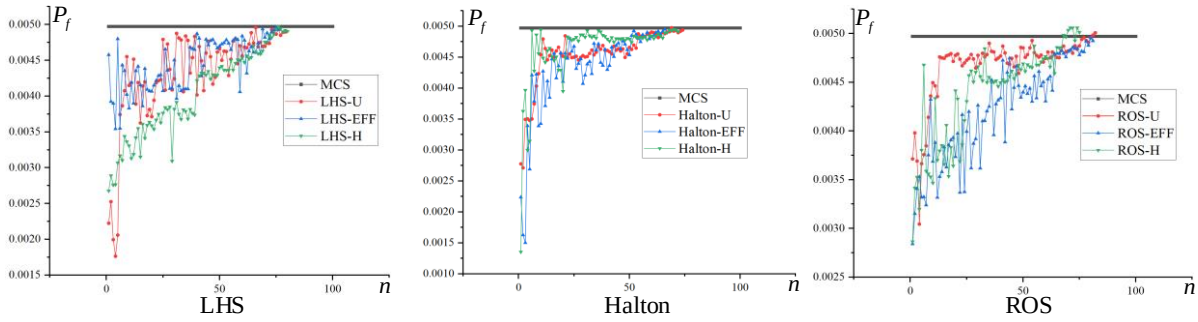

Figure. 15. Failure probability iteration diagram of supporting bracket engineering example

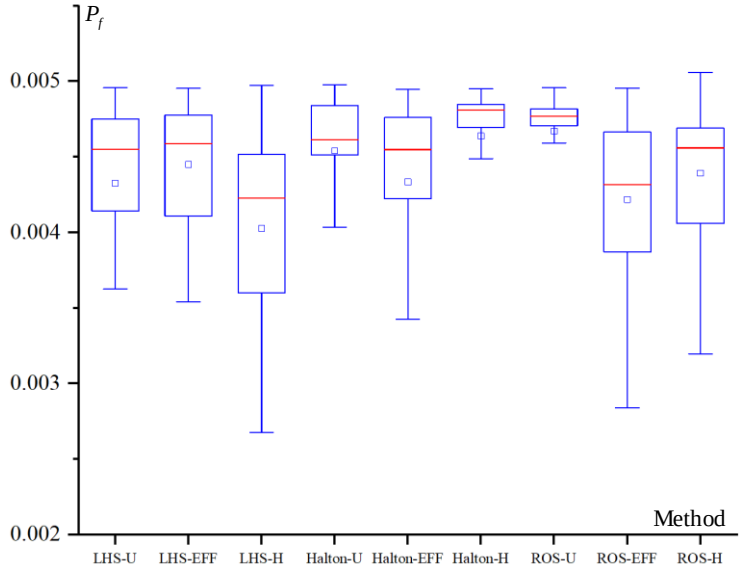

Figure. 16. Boxplot of failure probability of support bracket engineering example

Table 7 Calculation results of supporting bracket engineering example considering random uncertainties

Method	n	P_f	δ / %	**Method**	n	P_f	δ / %
MCS	2×10^6	0.004972	0	Halton-U	12+74	0.004940	0.6
LHS-H	12+80	0.004907	1.3	Halton-EFF	12+66	0.004949	0.5
LHS-U	12+79	0.004897	1.5	ROS-H	12+75	0.005014	0.8
LHS-EFF	12+76	0.004928	0.9	ROS-U	12+82	0.005009	0.7
Halton -H	12+72	0.004915	1.1	ROS-EFF	12+81	0.004925	0.9

As shown in Figure 15, the calculation results of the failure probabilities of each combination converge regularly around the MCS from small to large. According to the comparison of the results in Table 7, if only the learning function is compared, it can be seen that the calculation accuracy of the combination corresponding to the EFF function is the highest and the number of iterations is the least. If only the sampling methods are compared, it can be seen

that the calculation accuracy of the combination corresponding to Halton low-difference sequence sampling is the highest and the number of iterations is the least. Comprehensively comparing all the data, it is considered that Halton-EFF has the best performance in this engineering example combination.

4.1.6 Square tube

This example is a thermal-mechanical coupling simulation example. As shown in Figure 17, it is a square tube for transporting certain materials in a food processing plant and the material is structural steel. The temperature on one side of the pipe is 30° and the fixed support is loaded. The temperature on the other side is T (T>30°) and the tensile force F is applied. The results obtained by finite element simulation analysis are shown in Figure 18. In this calculation example, the section outer width L and section inner width length D of the square tube section, the length H of the square tube, the temperature T and the tensile force F are five independent random variables. The distribution rules are shown in Table 8. The corresponding LSF are as follows:

$$G(L,D,H,T,F)=[\sigma]-\sigma_{\max}(L,D,H,T,F) \tag{33}$$

where $[\sigma]$ is the yield strength of the structural steel. $\sigma_{\max}$ represents the actual maximum equivalent stress, which is an implicit function of L,H,D,T,F . The calculation results are shown in Table 9. The iteration plot and box plot of the failure probability are shown in Figure 19 and Figure 20 respectively.

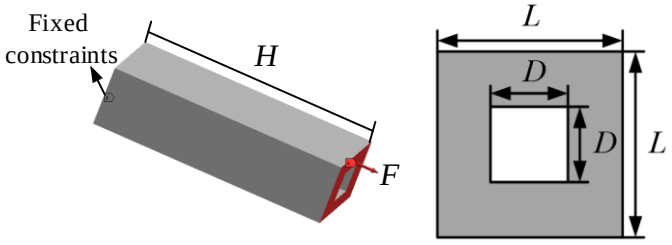

Figure. 17. Square tube modeling

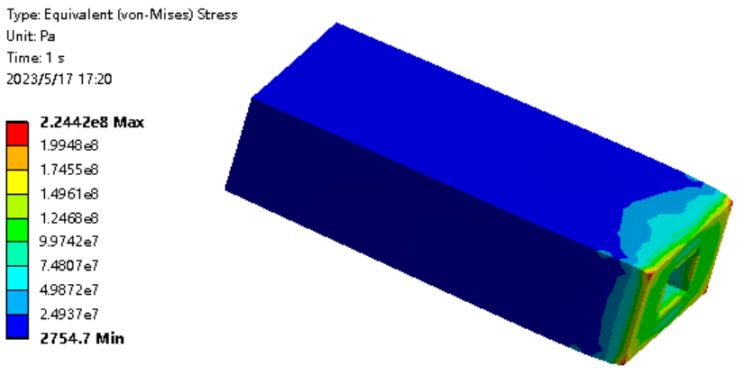

Figure. 18. ANSYS simulation results

Table 8 Variable information of square tube example

Variable	Distribution	Mean	Standard deviation
Section outer width L/mm	Normal	200	7
Section inner width D/mm	Normal	75	2.5
Tube length H/mm	Normal	400	13
Temperature T /□	Normal	50	2
Force F/N	Normal	50	2

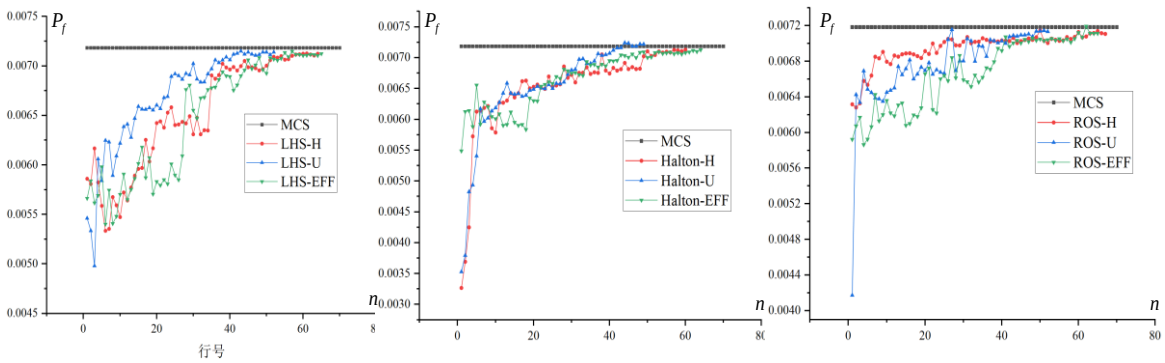

LHS Halton ROS

Figure. 19. Failure probability iteration diagram of square tube engineering example

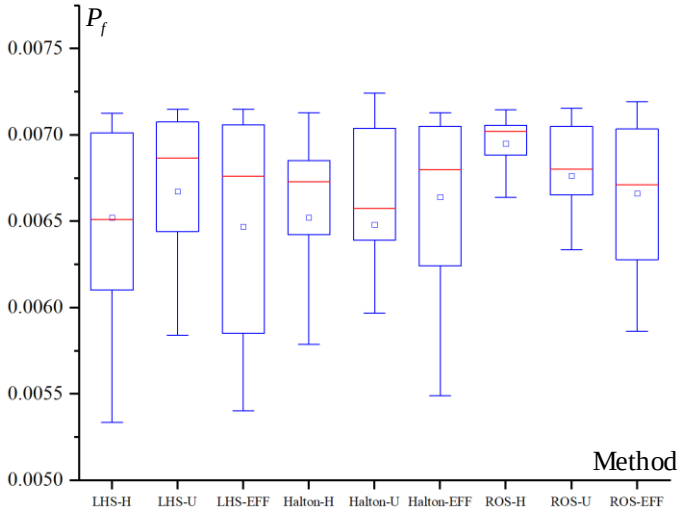

Figure. 20. Failure probability boxplot of square tube engineering example

Table 9 Calculation results of square tube engineering example considering random uncertainties

Method	n	P_f	δ / %	**Method**	n	P_f	δ / %
MCS	2×10^6	0.007184	0	Halton-U	12+49	0.007220	0.5
LHS-H	12+64	0.007124	0.8	Halton-EFF	12+64	0.007129	0.7
LHS-U	12+52	0.007140	0.6	ROS-H	12+67	0.007109	1.0
LHS-EFF	12+65	0.007125	0.8	ROS-U	12+52	0.007135	0.7
Halton -H	12+60	0.007130	0.7	ROS-EFF	12+65	0.007114	1.0

As shown in Figure 19, the calculation results of the failure probabilities of each combination converge regularly around the MCS from small to large, which again shows that the learning function also has a certain effect on the reliability analysis of engineering practice. According to the comparison of the results in Table 9, the number of iterations of the overall learning function has been reduced. If only the learning function is compared, it can be seen that the calculation accuracy of the combination corresponding to the U function is the highest and the number of iterations is the least. If only the sampling is compared method, it can be seen that the calculation accuracy of the combination corresponding to Halton low-difference sequence sampling is the highest and the number of iterations is the least. Comprehensively comparing all the data, it is considered that Halton-U is the combination with the best performance in this engineering example.

4.1.7 Results and discussion

ASVM-MCS has a very good effect in classical probabilistic reliability analysis, not only with higher accuracy, but also far more efficient than MCS; Among the three learning functions, the calculation accuracy of the results corresponding to the EFF function is higher and the number of iterations is less; In the three sampling methods, Halton low-bias sequence sampling corresponds to higher calculation accuracy and fewer iterations; Halton-EFF has the best performance in the nine ASVM classic probabilistic reliability analysis combination.

4.2 Numerical examples for the comparative study on hybrid ASVM-MCS framework considering mixed uncertainties

The problem of probability interval mixed reliability analysis has always been a concern in engineering practice due to the presence of interval variables [47-53]. This section also provides three numerical examples and three engineering examples to comparatively study the performance of the hybrid ASVM-MCS framework considering mixed uncertainties.

4.2.1 Nonlinear function

Similar to the nonlinear function calculation example in Section 4.1.1, an interval variable is added on the basis of it. The LHS can be expressed as:

$$f(x) = 11 - 0.1x_1^3 - x_2^2 - x_3 \tag{34}$$

where x_1 and x_2 are independent probability variables, both of which obey $N(0,1)$. x_3 is an independent interval variable. Its range is $[-3,3]$. The calculation results of each combination are shown in Table 10. The iteration diagram and box diagram of the failure probability are shown in Figure 21 and Figure 22 respectively:

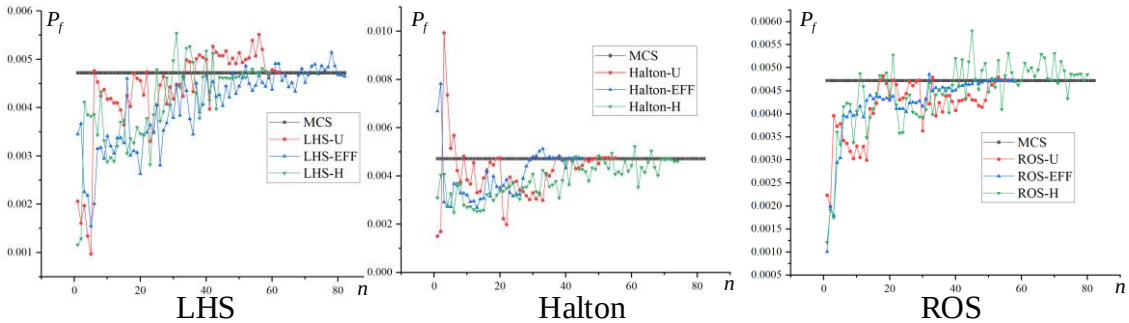

Figure. 21. Iteration diagram of maximum failure probability for nonlinear function example

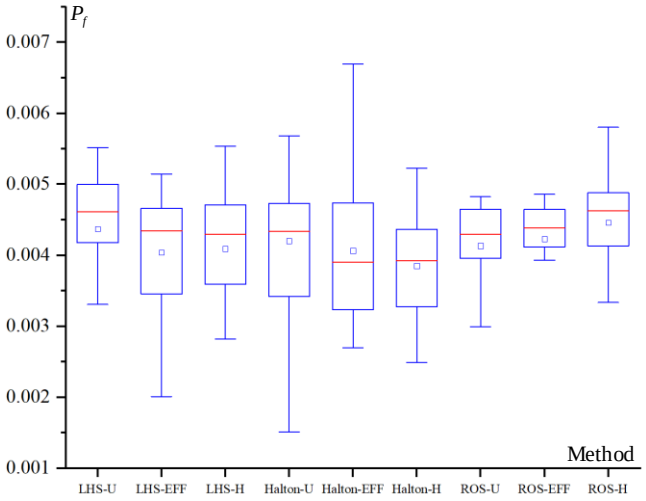

Figure. 22. Boxplot of maximum failure probability for nonlinear function example

Table 10 Calculation results of nonlinear function example considering mixed uncertainties

Method	n	P_f	δ / %	**Method**	n	P_f	δ / %
MCS	200×10^6	0.004722	0	Halton-U	12+55	0.004754	0.7
LHS-H	12+59	0.004713	0.2	Halton-EFF	12+45	0.004735	0.3
LHS-U	12+62	0.004736	0.3	ROS-H	12+80	0.004856	2.8
LHS-EFF	12+82	0.004651	1.5	ROS-U	12+56	0.004734	0.3
Halton-H	12+74	0.004609	2.4	ROS-EFF	12+58	0.004700	0.5

Among them, for MCS, the n means that the interval variable takes 200 sample points and the probability variable takes 10^6 sample points for nested simulation calculation. For various combinations, it means the initial sample point 12 plus the number of iterations of the learning function.

It can be seen from Figure 21 that the failure probabilities of most combinations gradually converge to near the MCS with the optimization iteration of the learning function from small to large, while the LHS-U combination exceeds the MCS in most cases. However, the results ultimately converged to MCS. It can be seen that in the probability-interval mixed reliability analysis, the adaptive support vector machine can still have a good effect. It can be seen from Table 10 that the calculation results of each combination are still within the error range. If only the learning function is compared, it can be seen that the calculation accuracy corresponding to the U function is relatively high and the number of iterations is also small. If only the sampling

methods are compared, it can be seen that the calculation accuracy corresponding to the Halton low-bias sequence sampling is relatively high and the number of iterations is also small. Comprehensively comparing all the results, the performance of the Halton-U combination is the best in this mixed reliability mathematical example.

4.2.2 Highly nonlinear function

Similar to the highly nonlinear function calculation example in Section 4.1.2, an interval variable is added on the basis of it. The LHS can be expressed as:

$$y = 1 + 1/256(x_1 + x_2 - 10)^4 - 10/(x_1 + x_2) + 0.1x_3 \tag{35}$$

where $x_1 \in N(10,3), x_2 \in N(10,3)$, and $x_3 \in [2,8]$. The calculation results of each combination are shown in Table 11. The iteration diagram and box diagram of the failure probability are shown in Figure 23 and Figure 24 respectively:

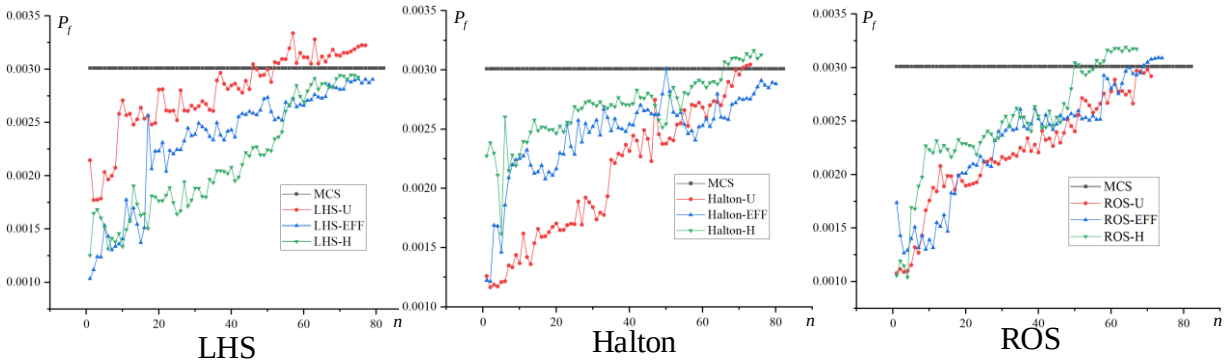

Figure. 23. Iteration diagram of maximum failure probability for highly nonlinear function example

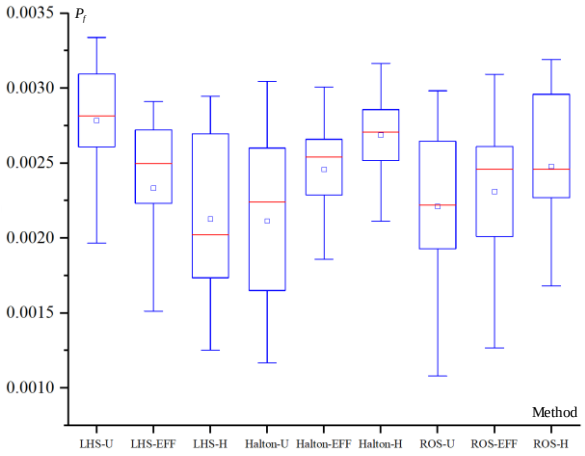

Figure. 24. Boxplot of maximum failure probability for highly nonlinear function example

Table 11 Calculation results of highly nonlinear function example considering mixed uncertainties

Method	n	P_f	δ / %	**Method**	n	P_f	δ / %

MCS	200×10^6	0.003011	0	Halton-U	12+73	0.003047	1.20
LHS-H	12+75	0.002927	2.79	Halton-EFF	12+80	0.002884	4.22
LHS-U	12+77	0.003125	3.79	ROS-H	12+67	0.003175	5.44
LHS-EFF	12+79	0.002905	3.52	ROS-U	12+71	0.002920	3.02
Halton-H	12+76	0.003129	3.92	ROS-EFF	12+74	0.003090	2.62

It can be seen from Figure 23 that the increase in the degree of nonlinearity does not affect ASVM, and the calculation results are still slowly approaching MCS. It can be seen from Table 11 that the calculation error is slightly increased compared with Table 2, but the effect is still objective. If only the sampling method is compared, the Halton low-bias sequence sampling has the highest precision and the fastest efficiency. if only the learning function is compared, the U function has the highest precision and the fastest efficiency. Comprehensive comparison shows that the Halton-U combination has the best performance.

4.2.3 High-dimensional nonlinear functions

By modifying the high-dimensional functional function in Section 4.1.3, two of the random variables are changed from probability variables to interval variables. The modified LHS can be expressed as:

$$f(x)=\sum_{i=1}^{19}\left[2(x_{i+1}-x_i^2)^2+0.5(x_i-1)^2\right]-600 \tag{36}$$

where $x_1,x_2,...,x_{18}$ are independent probability variables and they all obey $N(0,1)$. x_{19},x_{20} are mutually independent interval variables. Their range are $[-3,3]$. The calculation results are shown in Table 12. The iteration diagram and boxplot are shown in Figure 25 and Figure 26 respectively:

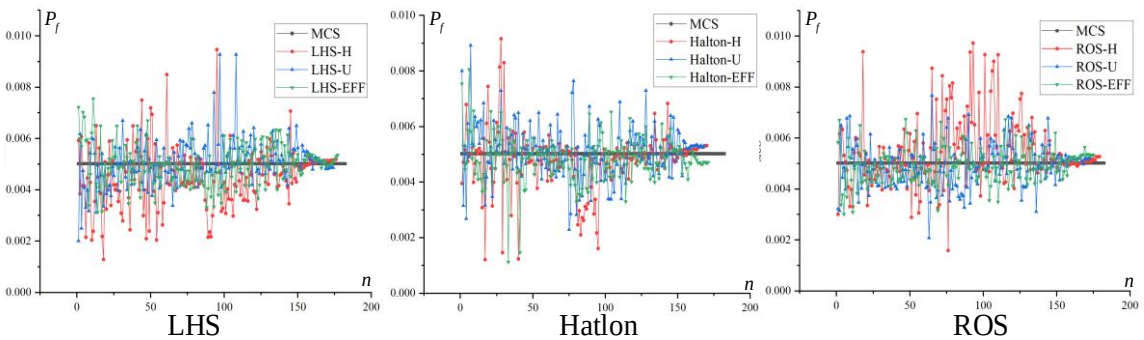

Figure. 25. Iteration diagram of maximum failure probability for high-dimensional nonlinear function example

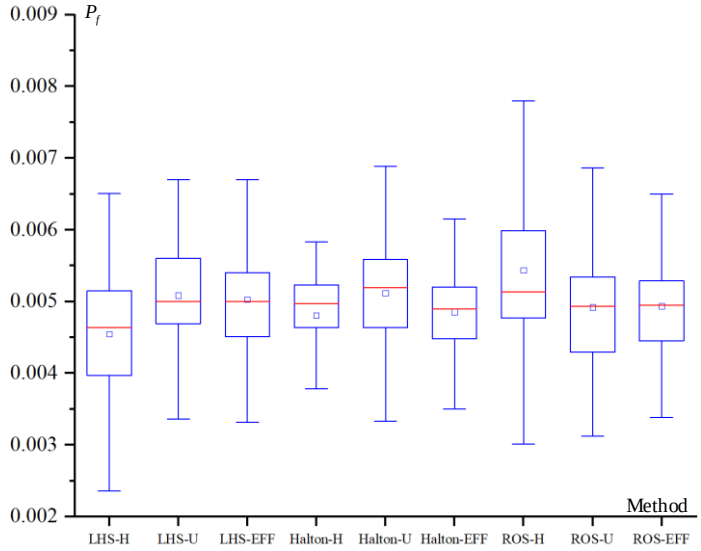

Figure. 26. Boxplot of maximum failure probability for high-dimensional nonlinear function example

Table 12 Calculation results of high-dimensional function example considering mixed uncertainties

Method	n	P_f	δ / %	**Method**	n	P_f	δ / %
MCS	200×10^6	0.005028	0	Halton-U	20+168	0.005312	5.6
LHS-H	20+176	0.005197	3.4	Halton-EFF	20+171	0.004720	6.1
LHS-U	20+174	0.004865	3.2	ROS-H	20+179	0.005278	4.8
LHS-EFF	20+177	0.005364	6.7	ROS-U	20+172	0.005228	4.0
Halton-H	20+170	0.005320	6.0	ROS-EFF	20+175	0.005330	6.0

As shown in Figure 25, which is similar to Figure 8, the calculation results of the failure probability of each combination fluctuated significantly, but eventually gradually converged near MCS. According to the comparison of the results in Table 12, the calculation accuracy of the results has increased to a certain extent compared with Table 3. If only the learning function is compared, it can be seen that the calculation accuracy of the corresponding combination of the U function is the highest and the number of iterations is the least. If only the sampling methods are compared, it can be seen that the calculation accuracy of the combination corresponding to Halton low-bias sequence sampling is the highest and the number of iterations is the least. Comprehensively comparing all the data, Halton-U is the combination with the best performance

in this high-dimensional example.

4.2.4 Cantilever Beam

This calculation example is modified on the basis of Section 4.1.4, changing L to an interval variable and $L \in [40,160]$.The corresponding LSF is as follows:

$$Z = D_0 - \frac{2L^3}{E\omega t}\sqrt{(\frac{P_x}{\omega^2})^2 + (\frac{P_y}{t^2})^2} \tag{37}$$

The calculation results of each combination are shown in Table 13. The iteration diagram and box plot of the failure probability are shown in Figure 27 and Figure 28 respectively.

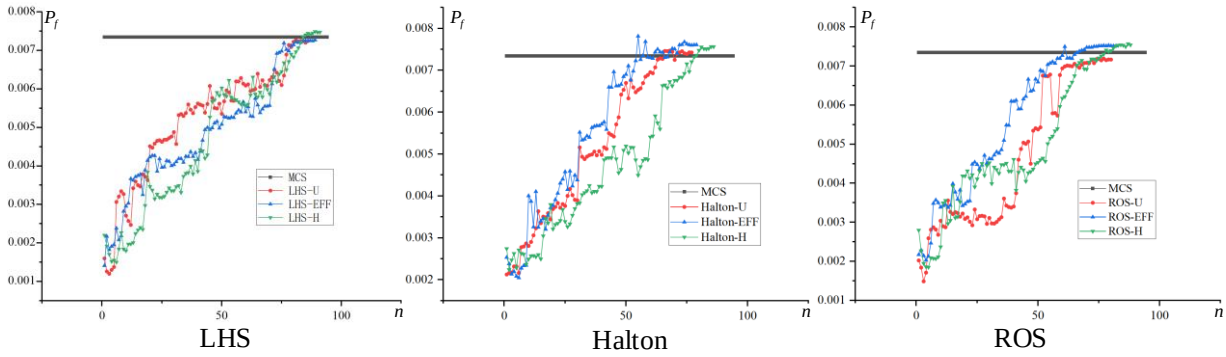

Figure. 27. Iterative diagram of maximum failure probability for cantilever beam engineering example

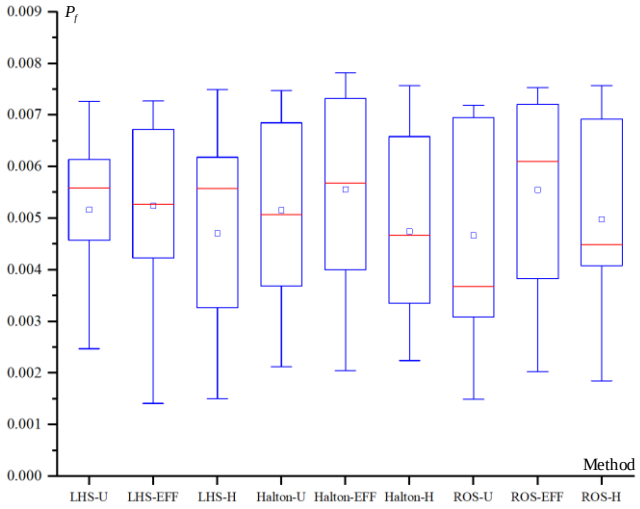

Figure. 28. Boxplot of maximum failure probability for cantilever beam engineering example

Table 13 Calculation result of cantilever beam engineering example considering mixed uncertainties

Method	n	P_f	δ / %	**Method**	n	P_f	δ / %
MCS	200×10^6	0.007348	0	Halton-U	12+77	0.007429	1.10
LHS-H	12+91	0.007481	1.81	Halton-EFF	12+79	0.007610	3.56

LHS-U	12+86	0.007248	1.36	ROS-H	12+88	0.007546	2.69
LHS-EFF	12+89	0.007273	1.02	ROS-U	12+82	0.007170	2.42
Halton-H	12+86	0.007568	2.99	ROS-EFF	12+82	0.007516	2.29

As shown in Figure 27, the calculation results of the failure probability of each combination fluctuated significantly, but eventually gradually converged near MCS. From the comparison of the results in Table 13, it can be seen that the calculation efficiency of the results is lower than that in Table 5, but the calculation accuracy is improved to a certain extent. If only the learning function is compared, it can be seen that the calculation accuracy of the corresponding combination of the U function is the highest and the number of iterations is the least. If only the sampling methods are compared, it can be seen that the calculation accuracy of the combination corresponding to Halton low-bias sequence sampling is the highest and the number of iterations is the least. Comprehensively comparing all the data, Halton-U is the combination with the best performance in this high-dimensional example.

4.2.5 Support bracket

The engineering calculation example of the supporting bracket in Section 4.1.5 is slightly modified. The thickness of the rib plate is changed from a probability variable to an interval variable. The variable distribution is shown in Table 14. The corresponding LHS is as follows:

$$G(L,H,D)=[\varepsilon]-\varepsilon_{\max}(L,H,D) \tag{38}$$

where $[\varepsilon]$ is the artificial maximum deformation limit value. $\varepsilon_{\max}$ represents the actual maximum equivalent total deformation, which is an implicit function of L,H,D and the unit is $10^{-6}m$. The calculation results of each combination are shown in Table 15. The iteration diagram and box plot of the failure probability are shown in Figure 29 and Figure 30 respectively.

Table 14 Variable information of support bracket example

Variable	Distribution	Parameter one	Parameter two
Rib length L/mm	Normal	30	1
Rib width H/mm	Normal	30	1

Rib thickness D/mm	Interval	2.2	2.8

For probability variables, parameter 1 and parameter 2 represent the mean and standard deviation respectively. for interval variables, parameter 1 and parameter 2 represent the lower bound and upper bound of the interval respectively. The following example also expresses this. No repeated explanation will be given later.

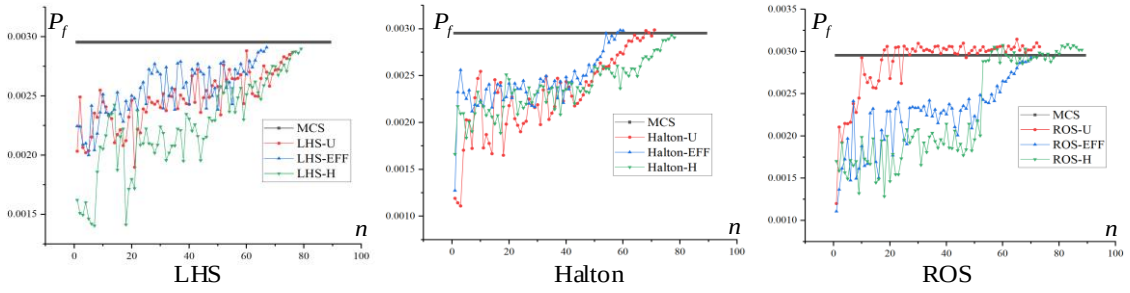

Figure. 29. Iterative diagram of maximum failure probability for support bracket engineering example

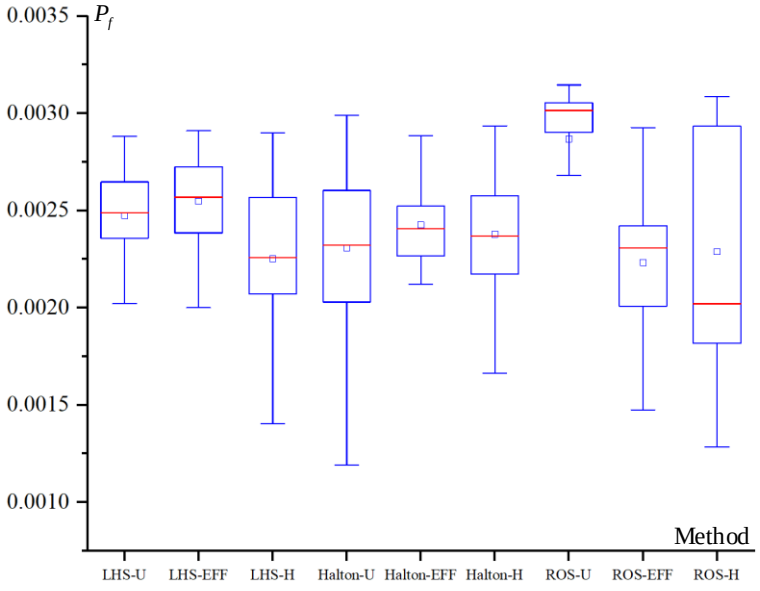

Figure. 30. Boxplot of maximum failure probability for support bracket engineering example

Table 15 Calculation result of support bracket engineering example

Method	n	P_f	δ / %	**Method**	n	P_f	δ / %
MCS	200×10^6	0.002955	0	Halton-U	12+71	0.002990	1.2
LHS-H	12+79	0.002900	1.9	Halton-EFF	12+60	0.002982	1.0
LHS-U	12+76	0.002869	2.9	ROS-H	12+87	0.003021	2.2
LHS-EFF	12+67	0.002911	1.5	ROS-U	12+73	0.003058	3.5

Halton-H	12+78	0.002908	1.6	ROS-EFF	12+70	0.002927	1.0

It can be seen from Figure 29 that the failure probability of most combinations gradually converges near the MCS with the optimization iteration of the learning function, while the result of the ROS-U combination exceeds the MCS early. But in the end, it still converges to MCS. The result of ROS-H combination starts to be far away from MCS, and then quickly starts to converge. It can also be seen from the mean values of failure probabilities in the convergence process of each combination in Figure 30 that the mean value of ROS-U far exceeds that of other combinations. It can be seen from Table 15 that each calculation error has increased to a certain extent compared with Table 7, but it is still within the error range. If only the learning function is compared, it can be seen that the calculation accuracy corresponding to the EFF function is higher and the number of iterations is less. Only by comparing the sampling method, it can be seen that the calculation accuracy corresponding to the Halton low-deviation sequence sampling is higher and the number of iterations is also less. Comparing all the results comprehensively, the performance of the Halton-EFF combination is the best in this mixed reliability engineering example.

4.2.6 Square tube

By slightly modifying the engineering calculation example of the square tube in Section 4.1.6, the tensile force F is changed from a probability variable to an interval variable. The variable distribution is shown in Table 16. Each variable is independent of each other. Through the finite element simulation again, the following LHS is obtained:

$$G(L,D,H,T,F)=[\sigma]-\sigma_{\max}(L,D,H,T,F) \tag{39}$$

where $[\sigma]$ is the yield strength of the structural steel $\sigma_{\max}$ represents the actual maximum equivalent stress. $\sigma_{\max}$ is an implicit function of L,H,D,T,F and its unit is $10^8 Pa$. The calculation results of each combination are shown in Table 17. The iteration diagram and box plot of the maximum failure probability are shown in Figure 31 and Figure 32 respectively:

Table 16 Variables information of square pipe engineering example

Variable	Distribution	Parameter one	Parameter two

Cross section length L/mm	Normal	200	7
Section inner width D/mm	Normal	75	2.5
Tube chief H/mm	Normal	400	13
Temperature T/℃	Normal	50	2
Force F/N	Interval	44	56

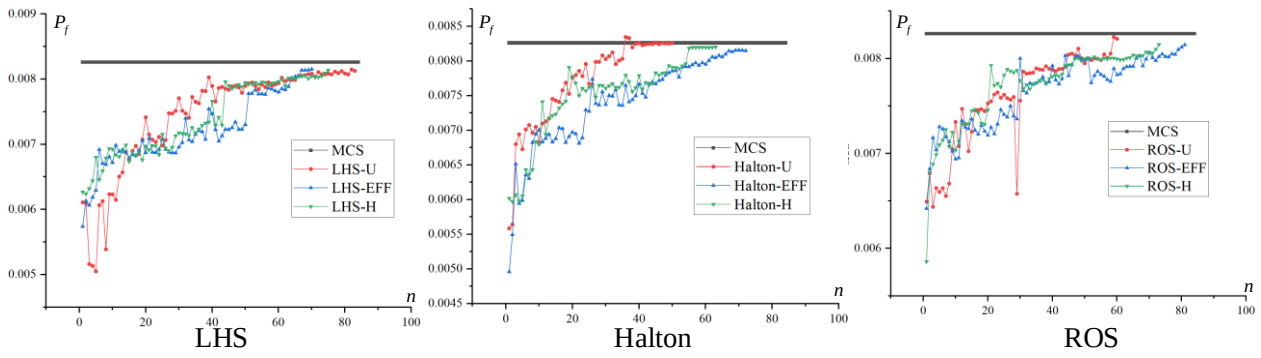

Figure. 31. The iterative diagram of the maximum failure probability for square tube engineering example

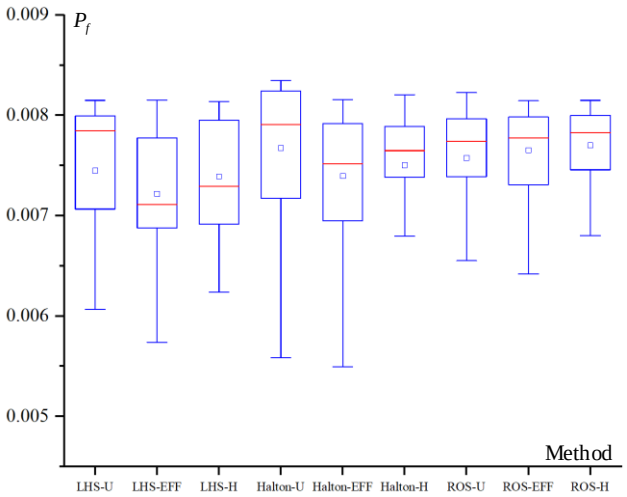

Figure. 32. Boxplot of maximum failure probability for cantilever beam engineering example square tube engineering example

Table 17 Calculation result of square tube engineering example

Method	n	P_f	δ / %	**Method**	n	P_f	δ / %
MCS	200×10^6	0.008263	0	Halton-U	12+50	0.008260	0.1
LHS-H	12+75	0.008139	1.5	Halton-EFF	12+72	0.008148	1.4

LHS-U	12+83	0.008129	1.6	ROS-H	12+73	0.008149	1.4
LHS-EFF	12+70	0.008153	1.3	ROS-U	12+60	0.008208	0.7
Halton-H	12+63	0.008205	0.7	ROS-EFF	12+81	0.008145	1.4

It can be seen from Figure 31 that the failure probabilities of all combinations gradually converge near the MCS with the optimization iteration of the learning function from small to large. It can be seen from Table 17 that each calculation error has increased to a certain extent compared with Table 9, but it is still within the error range. If only the learning function is compared, it can be seen that the U function has higher calculation accuracy and fewer iterations. If only the sampling methods are compared, it can be seen that Halton low-bias sequence sampling corresponds to higher calculation accuracy and fewer iterations. Comparing all the results comprehensively, the Halton-U combination performance is the best in this mixed reliability engineering example.

4.3 Numerical examples for the comparative study on system reliability based on hybrid adaptive framework

As structural systems are present in engineering practice, the study of reliability analysis for multiple failure modes is also a crucial research focus [54-58]. This section presents four engineering examples of series parallel systems and introduces interval variables for further comparative research.

4.3.1 System reliability analysis of probability variables based on ASVM-MCS

By modifying the engineering calculation example of the supporting bracket in Section 4.1.5, adding an equivalent stress as a dependent variable, and re-passing the finite element simulation to obtain the LSF as shown in Eq. (40), the two branches form a double failure mode system.

$$\begin{cases} G_1(L,H,D) = [\varepsilon] - \varepsilon_{\max}(L,H,D) \\ G_2(L,H,D) = [\sigma] - \sigma_{\max}(L,H,D) \end{cases} \tag{40}$$

where $[\varepsilon]$ is the artificial maximum deformation limit value. $[\sigma]$ is the yield strength of

structural steel. $\varepsilon_{\max}$ represents the maximum total deformation. $\sigma_{\max}$ represents the maximum equivalent stress. Both $\sigma_{\max}$ and $\varepsilon_{\max}$ are implicit functions on L, H, D.

4.3.1.1 Series system analysis

This engineering calculation example is constructed as a series failure mode system for calculation. The calculation results of each combination are shown in Table 18. The iteration diagram and box diagram of the failure probability are shown in Figure 33 and Figure 34 respectively:

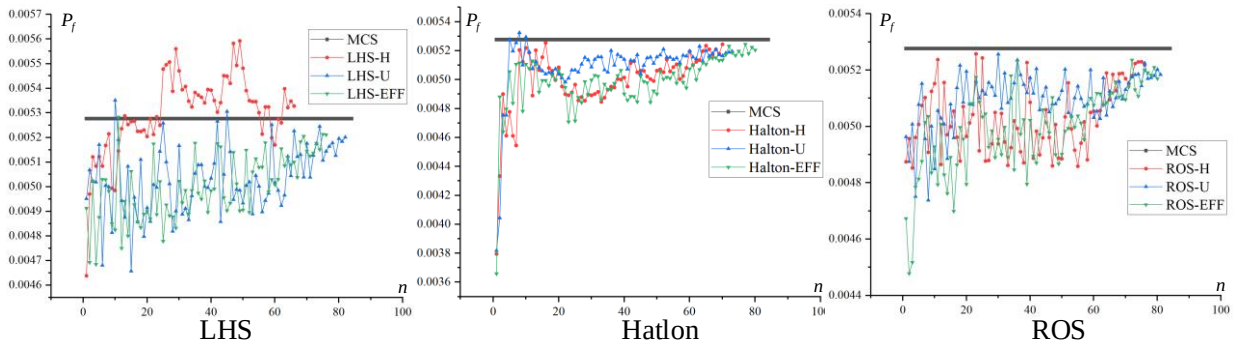

Figure. 33. Iteration diagram of failure probability of the series system for the support bracket engineering example

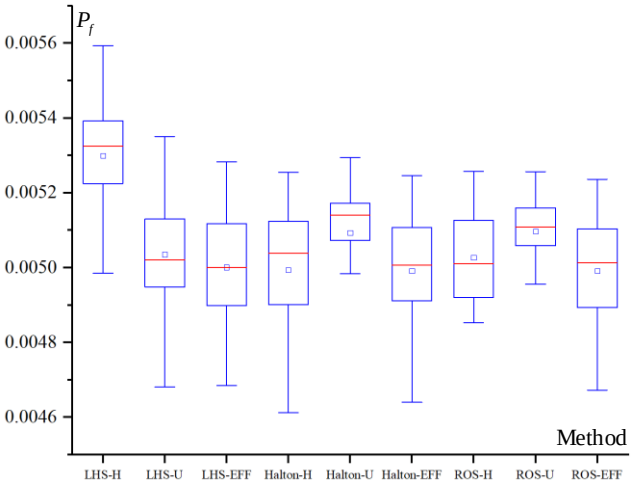

Figure. 34. Boxplot of failure probability of series system for support bracket engineering example

Table 18 Calculation results of series system of support bracket engineering example

Method	n	P_f	δ / %	**Method**	n	P_f	δ / %
MCS	2×10^6	0.005277	0	Halton-U	12+73	0.005195	1.6
LHS-H	12+66	0.005328	1.0	Halton-EFF	12+80	0.005205	1.4

LHS-U	12+82	0.005201	1.4	ROS-H	12+76	0.005219	1.1
LHS-EFF	12+76	0.005212	1.2	ROS-U	12+81	0.005184	1.8
Halton-H	12+70	0.005245	0.6	ROS-EFF	12+80	0.005170	2.0

As shown in Figure 33, the calculation results of the failure probabilities of each combination converge regularly around the MCS, indicating that ASVM still has a good effect on the probabilistic reliability analysis of series systems. According to the comparison of the results in Table 18, if only the learning function is compared, it can be seen that the calculation accuracy of the combination corresponding to the H function is the highest and the number of iterations is the least. If only the sampling methods are compared, it can be seen that the calculation accuracy of the combination corresponding to the Halton low-difference sequence sampling is the highest and the number of iterations is the least. Comparing all the data comprehensively, it is considered that Halton-H is the combination with the best performance in this parallel system engineering example.

4.3.1.2 Parallel system analysis

This engineering calculation example is constructed as a parallel failure mode system for calculation. The calculation results of each combination are shown in Table 19. The iteration diagram and box diagram of the failure probability are shown in Figure 35 and Figure 36 respectively:

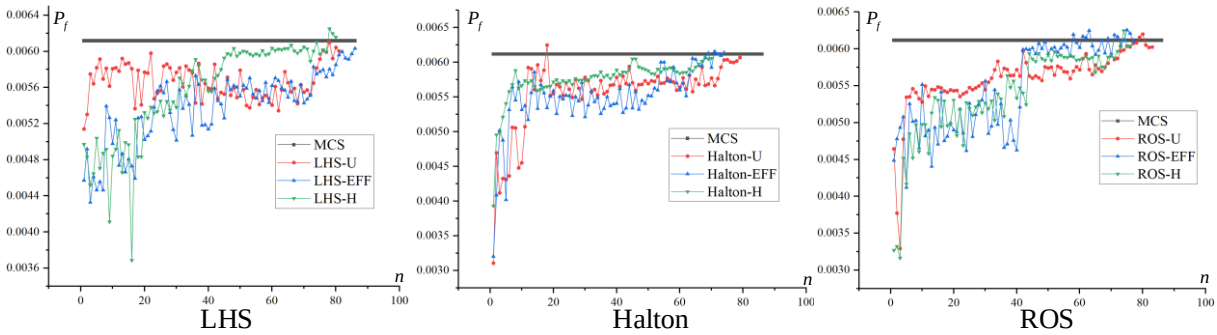

Figure. 35. Iteration diagram of failure probability of the series system for support bracket engineering example

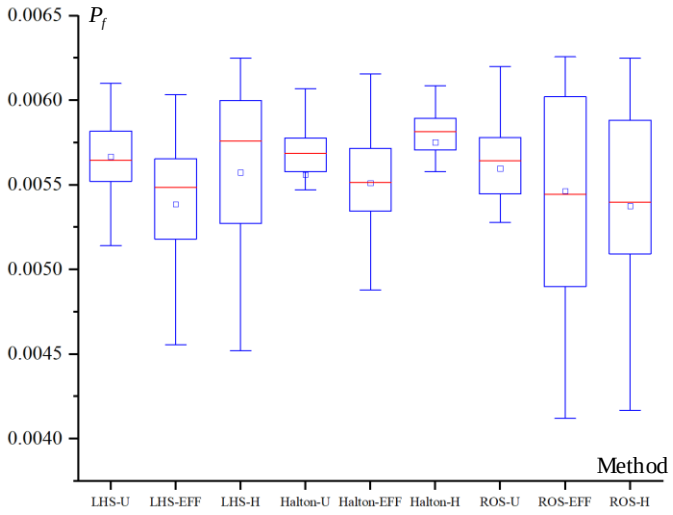

Figure. 36. Boxplot of failure probability of parallel system for support bracket engineering example

Table 19 Calculation results of parallel system of support bracket engineering example

Method	n	P_f	δ / %	**Method**	n	P_f	δ / %
MCS	2×10^6	0.006118	0	Halton-U	12+79	0.006070	0.78
LHS-H	12+80	0.006158	0.65	Halton-EFF	12+74	0.006140	0.36
LHS-U	12+81	0.006005	1.85	ROS-H	12+76	0.006042	1.24
LHS-EFF	12+86	0.006033	1.39	ROS-U	12+83	0.006026	1.50
Halton-H	12+70	0.006059	0.96	ROS-EFF	12+77	0.006106	0.20

As shown in Figure 35, the calculation results of the failure probabilities of each combination converge regularly around the MCS, indicating that ASVM also has a good effect on the probabilistic reliability analysis of parallel systems. According to the comparison of the results in Table 19, if only the learning function is compared, it can be seen that the calculation accuracy of the combination corresponding to the EFF function is the highest and the number of iterations is the least. If only the sampling methods are compared, it can be seen that the calculation accuracy of the combination corresponding to the Halton low-difference sequence sampling is the highest and the number of iterations is the least. Comparing all the data comprehensively, it is considered that Halton-EFF is the combination with the best performance in this parallel system engineering example.

4.3.2 System reliability analysis of mixed variables based on ASVM-MCS

By modifying the engineering calculation example of the supporting bracket in Section 4.2.5, an equivalent stress is added as a dependent variable. The LSF of Eq. (41) is obtained through finite element simulation again. The two branches form a dual failure mode system.

$$\begin{cases} G_1(L,H,D) = [\varepsilon] - \varepsilon_{\max}(L,H,D) \\ G_2(L,H,D) = [\sigma] - \sigma_{\max}(L,H,D) \end{cases} \tag{41}$$

4.3.2.1 Series system analysis

This engineering calculation example is constructed as a series failure mode system for calculation. The calculation results of each combination are shown in Table 20, and the iteration diagram and box diagram of the failure probability are shown in Figure 37 and Figure 38 respectively:

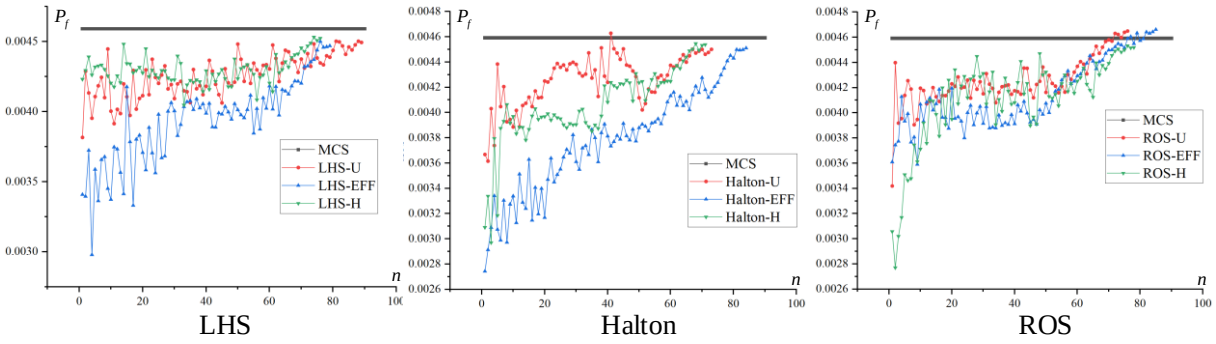

Figure. 37. Iteration diagram of the maximum failure probability of series system for support bracket engineering example

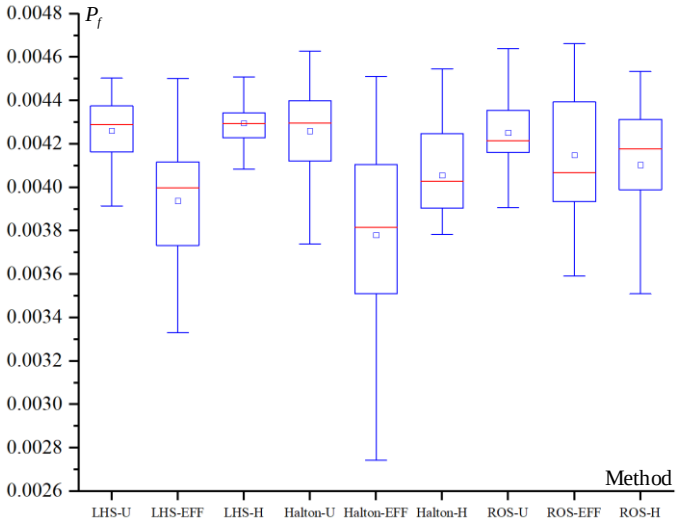

Figure. 38. Boxplot of maximum failure probability of series system for the support bracket engineering example

Table 20 Calculation results of series system of support bracket engineering example considering mixed uncertainties

Method	n	P_f	δ / %	**Method**	n	P_f	δ / %
MCS	200×10^6	0.004592	0	Halton-U	12+73	0.004501	2.0
LHS-H	12+76	0.004525	1.5	Halton-EFF	12+85	0.004511	1.8
LHS-U	12+89	0.004495	2.1	ROS-H	12+78	0.004520	1.6
LHS-EFF	12+79	0.004470	2.7	ROS-U	12+76	0.004650	1.3
Halton-H	12+71	0.004539	1.2	ROS-EFF	12+85	0.004662	1.5

As shown in Figure 37, the calculation results of the failure probabilities of each combination converge regularly around the MCS, indicating that ASVM still has a good effect on the probabilistic reliability analysis of series systems. According to the comparison of the results in Table 20, if only the learning function is compared, it can be seen that the calculation accuracy of the combination corresponding to the H function is the highest and the number of iterations is the least. If only the sampling methods are compared, it can be seen that the calculation accuracy of the combination corresponding to the Halton low-difference sequence sampling is the highest and the number of iterations is the least. Comparing all the data comprehensively, it is considered that Halton-H is the combination with the best performance in this series system hybrid reliability engineering example.

4.3.2.2 Parallel system analysis

This engineering calculation example is constructed as a parallel failure mode system for calculation. The calculation results of each combination are shown in Table 21. The iteration diagram and box diagram of the failure probability are shown in Figure 39 and Figure 40 respectively:

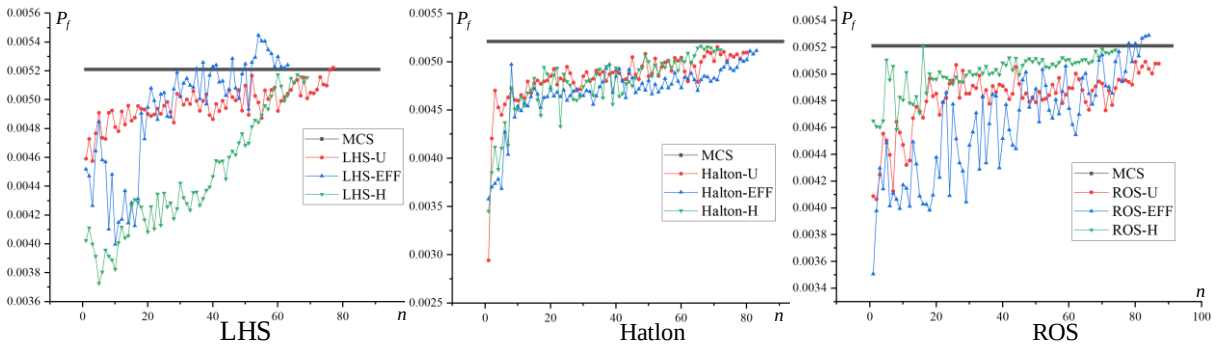

Figure. 39. Iteration diagram of the maximum failure probability of parallel system for support bracket engineering example

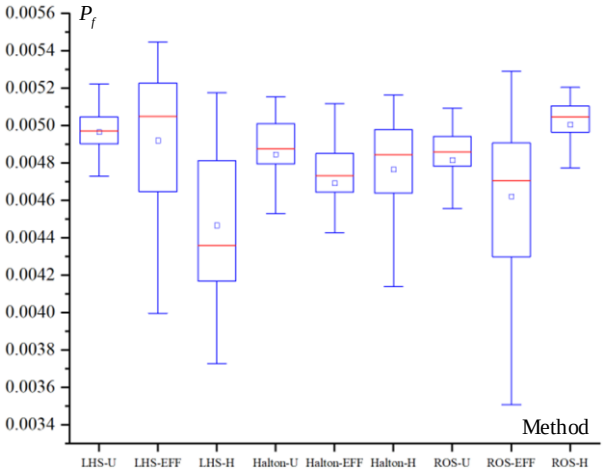

Figure. 40. Boxplot of maximum failure probability of parallel system for the support bracket engineering example

Table 21. Calculation results of parallel system of support bracket engineering example considering mixed uncertainties

Method	n	P_f	δ / %	**Method**	n	P_f	δ / %
MCS	200×10^6	0.005211	0	Halton-U	12+80	0.005098	2.2
LHS-H	12+69	0.005156	1.1	Halton-EFF	12+83	0.005117	1.8
LHS-U	12+77	0.005223	0.2	ROS-H	12+74	0.005181	0.6
LHS-EFF	12+63	0.005241	0.6	ROS-U	12+87	0.005079	2.5
Halton-H	12+72	0.005126	1.6	ROS-EFF	12+84	0.005290	1.5

As shown in Figure 39, the calculation results of the failure probabilities of each combination converge regularly around the MCS, indicating that ASVM also has a good effect

on the probability-interval hybrid reliability analysis of parallel systems. According to the comparison of the results in Table 21, if only the learning function is compared, it can be seen that the calculation accuracy of the combination corresponding to the H function is the highest and the number of iterations is the least. If only the sampling method is compared, it can be seen that the calculation accuracy of the combination corresponding to LHS is the highest and the number of iterations is the least. Comparing all the data comprehensively, it is considered that LHS-H is the combination with the best performance in this parallel system engineering example.

Comparing the results of four examples comprehensively, the Halton-H combination has the best performance in terms of system reliability.

5 Conclusion

Aiming at the problems and challenges in the structural reliability theory based on the surrogate model, this paper explores the reliability analysis method based on SVM. The main contents are as follows:

(1) Proposed the hybrid ASVM-MCS framework

Sampling techniques (LHS, Halton low-bias sequence sampling, ROS) are introduced to obtain a better initial sample set for SVM through more uniform sampling. By introducing intelligent optimization learning functions (U function, EFF, H function), selecting and updating sample points through specific formulas for iterative optimization, the prediction accuracy of the SVM model is increased. A variety of ASVM are constructed by combining them with each other.

(2) A comparative study: The proposed ASVM-MCS framework considering random uncertainties

Combining ASVM and MCS, and comparing the performance of multiple combinations through mathematical examples and engineering examples, this paper finally believes that Halton-EFF is the optimal combination for this type of problem

(3) A comparative study: The proposed ASVM-MCS framework considering mixed uncertainties

Combining ASVM with MCS, and comparing the performance of multiple combinations through mathematical examples and engineering examples, this paper finally believes that

Halton-U is the optimal combination for this type of problem.

(4) A comparative study: The proposed ASVM-MCS system reliability framework

Combining ASVM with MCS, and comparing the performance of multiple combinations through series-parallel probability and hybrid system engineering examples, this paper finally believes that Halton-H is the optimal combination for this type of problem.

Acknowledgments

This research was funded by the National Natural Science Foundation of China (Grant No. 12232004), the Sichuan Science and Technology Program (Grants No. 2022YFQ0087 and 2022JDJQ0024), the China Postdoctoral Science Foundation (Grant No. 2021M700693), and the Guangdong Basic and Applied Basic Research Foundation (Grant No. 2022A1515240010).

References

[1] Keshtegar, B., & Meng, Z. (2017). A hybrid relaxed first-order reliability method for efficient structural reliability analysis. *Structural Safety*, *66*, 84-93.

[2] Meng, Z., Li, G., Yang, D., & Zhan, L. (2017). A new directional stability transformation method of chaos control for first order reliability analysis. *Structural and Multidisciplinary Optimization*, 55, 601-612.

[3] Li, X. Q., Song, L. K., & Bai, G. C. (2022). Recent advances in reliability analysis of aeroengine rotor system: a review. *International Journal of Structural Integrity*, 13(1), 1-29.

[4] Meng, D., Yang, S., Lin, T., Wang, J., Yang, H., & Lv, Z. (2022). RBMDO using gaussian mixture model-based second-order mean-value saddlepoint approximation. *CMES-Computer Modeling in Engineering and Sciences*, 132(2), 553-568

[5] Mohamad Suffian, M. S. Z., Kamil, S., & Ariffin, A. K. (2022). Uncertainty analysis of varied meshes of a finite element model using Monte Carlo simulation. *International Journal of Structural Integrity*, 13(6), 907-921.

[6] Luo, C., Keshtegar, B., Zhu, S. P., Taylan, O., & Niu, X. P. (2022). Hybrid enhanced Monte Carlo simulation coupled with advanced machine learning approach for accurate and efficient structural reliability analysis. *Computer Methods in Applied Mechanics and Engineering*, 388, 114218.

[7] Tabandeh, A., Jia, G., & Gardoni, P. (2022). A review and assessment of importance sampling methods for reliability analysis. *Structural Safety, 97*, 102216.

[8] Xiao, S., Oladyshkin, S., & Nowak, W. (2020). Reliability analysis with stratified

importance sampling based on adaptive Kriging. *Reliability Engineering & System Safety*, 197, 106852.

[9] Jafari-Asl, J., Seghier, M. E. A. B., Ohadi, S., Correia, J., & Barroso, J. (2022). Reliability analysis based improved directional simulation using Harris Hawks optimization algorithm for engineering systems. *Engineering Failure Analysis*, 135, 106148.

[10] Zhang, X., Lu, Z., & Cheng, K. (2021). AK-DS: An adaptive Kriging-based directional sampling method for reliability analysis. *Mechanical Systems and Signal Processing*, 156, 107610.

[11] Schuëller, G. I., Pradlwarter, H. J., & Koutsourelakis, P. S. (2004). A critical appraisal of reliability estimation procedures for high dimensions. *Probabilistic engineering mechanics*, 19(4), 463-474.

[12] Pradlwarter, H. J., Pellissetti, M. F., Schenk, C. A., Schueller, G. I., Kreis, A., Fransen, S., & Klein, M. (2005). Realistic and efficient reliability estimation for aerospace structures. *Computer Methods in Applied Mechanics and Engineering*, 194(12-16), 1597-1617.

[13] Li, H. S., Ma, Y. Z., & Cao, Z. (2015). A generalized Subset Simulation approach for estimating small failure probabilities of multiple stochastic responses. *Computers & Structures*, 153, 239-251.

[14] Yang, S., Meng, D., Wang, H., Chen, Z., & Xu, B. (2023). A comparative study for adaptive surrogate-model-based reliability evaluation method of automobile components. *International Journal of Structural Integrity*. 14(3), 498-519.

[15] Wang, Y. H., Zhang, C., Su, Y. Q., Shang, L. Y., & Zhang, T. (2019). Structure optimization of the frame based on response surface method. *International Journal of Structural Integrity*, 11(3), 411-425.

[16] Roussouly, N., Petitjean, F., & Salaun, M. (2013). A new adaptive response surface method for reliability analysis. *Probabilistic Engineering Mechanics*, 32, 103-115.

[17] Li, H. S., Zhao, A. L., & Tee, K. F. (2016). Structural reliability analysis of multiple limit state functions using multi-input multi-output support vector machine. *Advances in Mechanical Engineering*, 8(10), 1687814016671447.

[18] Luo, C., Keshtegar, B., Zhu, S. P., & Niu, X. (2022). EMCS-SVR: Hybrid efficient and accurate enhanced simulation approach coupled with adaptive SVR for structural reliability analysis. *Computer Methods in Applied Mechanics and Engineering*, 400, 115499.

[19] Bourinet, J. M. (2016). Rare-event probability estimation with adaptive support vector regression surrogates. *Reliability Engineering & System Safety*, 150, 210-221.

[20] Lins, I. D., Moura, M. D. C., Zio, E., & Droguett, E. L. (2012). A particle swarm optimized support vector machine for reliability prediction. *Quality and Reliability Engineering International*, 28(2), 141-158.

[21] Luo, C., Zhu, S. P., Keshtegar, B., Niu, X., & Taylan, O. (2023). An enhanced uniform simulation approach coupled with SVR for efficient structural reliability analysis. *Reliability Engineering & System Safety*, 109377.

[22] Hong, W. C., & Pai, P. F. (2006). Predicting engine reliability by support vector machines. *The International Journal of Advanced Manufacturing Technology*, 28, 154-161.

[23] Echard, B., Gayton, N., Lemaire, M., & Relun, N. (2013). A combined importance sampling and kriging reliability method for small failure probabilities with time-demanding numerical models. *Reliability Engineering & System Safety*, 111, 232-240.

[24] Yu, S., Wang, Z., & Li, Y. (2022). Time and space-variant system reliability analysis through adaptive Kriging and weighted sampling. *Mechanical Systems and Signal Processing*, 166, 108443.

[25] Echard, B., Gayton, N., & Lemaire, M. (2011). AK-MCS: an active learning reliability method combining Kriging and Monte Carlo simulation. *Structural Safety*, 33(2), 145-154.

[26] Wang, Z., & Shafieezadeh, A. (2019). ESC: an efficient error-based stopping criterion for kriging-based reliability analysis methods. *Structural and Multidisciplinary Optimization*, 59, 1621-1637.

[27] Yang, M., Zhang, D., Wang, F., & Han, X. (2022). Efficient local adaptive Kriging approximation method with single-loop strategy for reliability-based design optimization. *Computer Methods in Applied Mechanics and Engineering*, 390, 114462.

[28] Yang, M., Zhang, D., Jiang, C., Han, X., & Li, Q. (2021). A hybrid adaptive Kriging-based single loop approach for complex reliability-based design optimization problems. *Reliability Engineering & System Safety*, 215, 107736.

[29] Meng, D., Yang, S., de Jesus, A. M., & Zhu, S. P. (2023). A novel Kriging-model-assisted reliability-based multidisciplinary design optimization strategy and its application in the offshore wind turbine tower. *Renewable Energy*, 203, 407-420.

[30] Meng, D., Yang, S., De Jesus, A. M., Fazeres-Ferradosa, T., & Zhu, S. P. (2023). A novel hybrid adaptive Kriging and water cycle algorithm for reliability-based design and optimization strategy: Application in offshore wind turbine monopile. *Computer Methods in Applied Mechanics and Engineering*, 412, 116083.

[31] Yu, S., & Li, Y. (2021). Active learning Kriging model with adaptive uniform design for time-dependent reliability analysis. *IEEE Access*, 9, 91625-9163.

[32] Meng, Z., Li, G., Wang, X., Sait, S. M., & Yıldız, A. R. (2021). A comparative study of metaheuristic algorithms for reliability-based design optimization problems. *Archives of Computational Methods in Engineering*, 28(3), 1853-1869.

[33] Li, C., Li, Y., Gao, L., Garg, A., & Li, W. (2021). Surrogate model‐based heat dissipation optimization of air‐cooling battery packs involving herringbone fins. *International Journal of Energy Research*, 45(6), 8508-8523.

[34] Ai, Q., Yuan, Y., Jiang, X., Wang, H., Han, C., Huang, X., & Wang, K. (2022). Pathological diagnosis of the seepage of a mountain tunnel. *Tunnelling and Underground Space Technology*, 128, 104657.

[35] Xue, Y., & Deng, Y. (2022). Extending set measures to orthopair fuzzy sets. *International Journal of Uncertainty Fuzziness and Knowledge-Based Systems*, 30(1), 63-91.

[36] Wang, Z., Xiao, F., & Cao, Z. (2022). Uncertainty measurements for Pythagorean fuzzy set and their applications in multiple-criteria decision making. *Soft Computing*, 26(19), 9937-9952.

[37] Rocco, C. M., & Moreno, J. A. (2002). Fast Monte Carlo reliability evaluation using support vector machine. *Reliability Engineering & System Safety*, 76(3), 237-243.

[38] Guo, Z., & Bai, G. (2009). Application of least squares support vector machine for regression to reliability analysis. *Chinese Journal of Aeronautics*, 22(2), 160-166.

[39] Pan, Q., & Dias, D. (2017). An efficient reliability method combining adaptive support vector machine and Monte Carlo simulation. *Structural Safety*, 67, 85-95.

[40] Cortes, C., & Vapnik, V. (1995). Support-vector networks. *Machine learning*, 20, 273-297.

[41] Niederreiter, H. (1988). Low-discrepancy and low-dispersion sequences. *Journal of number theory*, 30(1), 51-70.

[42] Echard, B., Gayton, N., & Lemaire, M. (2011). AK-MCS: an active learning reliability method combining Kriging and Monte Carlo simulation. *Structural Safety*, 33(2), 145-154.

[43] Bichon, B. J., Eldred, M. S., Swiler, L. P., Mahadevan, S., & McFarland, J. M. (2008). Efficient global reliability analysis for nonlinear implicit performance functions. *AIAA journal*, 46(10), 2459-2468.

[44] Lv, Z., Lu, Z., & Wang, P. (2015). A new learning function for Kriging and its applications to solve reliability problems in engineering. *Computers & Mathematics with Applications*, 70(5), 1182-1197.

[45] Xiao, N. C., Zuo, M. J., & Zhou, C. (2018). A new adaptive sequential sampling method to construct surrogate models for efficient reliability analysis. *Reliability Engineering & System Safety*, 169, 330-338.

[46] Zhang, J., Xiao, M., Gao, L., & Fu, J. (2018). A novel projection outline based active

learning method and its combination with Kriging metamodel for hybrid reliability analysis with random and interval variables. Computer methods in applied mechanics and engineering, 341, 32-52.

[47] Li, W., Li, C., Gao, L., & Xiao, M. (2020). Risk-based design optimization under hybrid uncertainties. *Engineering with Computers*, 38, 2037-2049.

[48] Meng, Z., Pang, Y., Pu, Y., & Wang, X. (2020). New hybrid reliability-based topology optimization method combining fuzzy and probabilistic models for handling epistemic and aleatory uncertainties. *Computer Methods in Applied Mechanics and Engineering*, 363, 112886.

[49] Liu, G., Xiao, F., Lin, C. T., & Cao, Z. (2020). A fuzzy interval time-series energy and financial forecasting model using network-based multiple time-frequency spaces and the induced-ordered weighted averaging aggregation operation. *IEEE Transactions on Fuzzy Systems*, 28(11), 2677-2690.

[50] Luo, Y., Kang, Z., & Li, A. (2009). Structural reliability assessment based on probability and convex set mixed model. *Computers & Structures*, 87(21-22), 1408-1415.

[51] Kang, Z., & Luo, Y. (2010). Reliability-based structural optimization with probability and convex set hybrid models. *Structural and Multidisciplinary Optimization*, 42, 89-102.

[52] Liu, X., Wang, X., Xie, J., & Li, B. (2020). Construction of probability box model based on maximum entropy principle and corresponding hybrid reliability analysis approach. Structural and Multidisciplinary Optimization, 61, 599-617.

[53] Liu, X., Li, T., Zhou, Z., & Hu, L. (2022). An efficient multi-objective reliability-based design optimization method for structure based on probability and interval hybrid model. *Computer Methods in Applied Mechanics and Engineering*, 392, 114682.

[54] Meng, D., Yang, S., He, C., Wang, H., Lv, Z., Guo, Y., & Nie, P. (2022). Multidisciplinary design optimization of engineering systems under uncertainty: a review. *International Journal of Structural Integrity*, 13(4), 565-593.

[55] Meng, D., Li, Y., He, C., Guo, J., Lv, Z., & Wu, P. (2021). Multidisciplinary design for structural integrity using a collaborative optimization method based on adaptive surrogate modelling. *Materials & Design*, 206, 109789.

[56] Zhu, S. P., Keshtegar, B., Tian, K., & Trung, N. T. (2021). Optimization of load-carrying hierarchical stiffened shells: comparative survey and applications of six hybrid heuristic models. *Archives of Computational Methods in Engineering*, 28(5), 4153-4166.

[57] Gao, X., Su, X., Qian, H., & Pan, X. (2022). Dependence assessment in human reliability analysis under uncertain and dynamic situations. *Nuclear Engineering and Technology*, 54(3), 948-958.

[58] Teng, D., Feng, Y. W., Chen, J. Y., & Lu, C. (2022). Structural dynamic reliability analysis: review and prospects. *International Journal of Structural Integrity*, 13(5),753-783.